



Contribution to the Theme Section 'Latest advances in research on fish early life stages'

Fine-scale larval fish distributions and predator–prey dynamics in a coastal river-dominated ecosystem

Kelia E. Axler^{1,6,*}, Su Sponaugle¹, Christian Briseño-Avena^{2,7},
Frank Hernandez Jr.³, Sally J. Warner^{4,8}, Brian Dzwonkowski⁵, Steven L. Dykstra⁵,
Robert K. Cowen²

¹Department of Integrative Biology, Hatfield Marine Science Center, Oregon State University, Newport, OR 97365, USA

²Hatfield Marine Science Center, Oregon State University, Newport, OR 97365, USA

³Division of Coastal Sciences, Gulf Coast Research Laboratory, University of Southern Mississippi, Ocean Springs, MS 39564, USA

⁴College of Earth, Ocean, and Atmospheric Sciences, Oregon State University, Corvallis, OR 97331, USA

⁵Department of Marine Sciences, University of South Alabama, Dauphin Island Sea Lab, Dauphin Island, AL 36528, USA

⁶Present address: Alaska Fisheries Science Center, National Oceanic and Atmospheric Administration, 7600 Sand Point Way, Seattle, WA 98115, USA

⁷Present address: Department of Environmental and Ocean Sciences, University of San Diego, San Diego, CA 92110, USA

⁸Present address: Environmental Studies Program, Brandeis University, Waltham, MA 02453, USA

ABSTRACT: River plumes discharging into continental shelf waters have the potential to influence the distributions, predator–prey relationships, and thus survival of nearshore marine fish larvae, but few studies have been able to characterize the plume environment at sufficiently fine scales to resolve the underlying mechanisms. We used a high-resolution plankton imaging system and a sparse convolutional neural network to automate image classification of larval fishes, their planktonic prey (calanoid copepods), and gelatinous planktonic predators (ctenophores, hydromedusae, and siphonophores) over broad spatial scales (km) and multiple pulses of estuarine water exiting Mobile Bay (Alabama, USA) into the northern Gulf of Mexico from 9–11 April 2016. Fine-scale (1 m) plankton distributions were examined to analyze predator–prey relationships across 3 distinct plume regimes that varied by degree of wind-forcing and mixing rates. In calm wind conditions, the water column was highly stratified, and fish larvae and zooplankton were observed aggregating in a region of river plume-derived hydrodynamic convergence. As winds strengthened, the water column was subjected to downwelling and highly turbulent conditions, and there was decreasing spatial overlap between larval fishes and their zooplankton prey and predators. Our results indicate that high-discharge plume regimes characterized by strong wind-forcing and turbulence can rapidly shift the physical and trophic environments from favorable to unfavorable for fish larvae. Multiple pathways for both nearshore retention and advective dispersal of fish larvae were also identified. Documenting this variability is a first step toward understanding how high discharge events and physical forcing can affect fisheries production in river-dominated coastal ecosystems worldwide.

KEY WORDS: Larval fish · River plumes · Fine scale · Predator–prey relationships

— Resale or republication not permitted without written consent of the publisher —

1. INTRODUCTION

Freshwater discharge into coastal oceans is an important biophysical driver of the distributions, transport, and survival of the early life stages of coastal

and estuarine fish assemblages (Grimes & Finucane 1991, Le Pape et al. 2003, Carassou et al. 2012). Although often only a few meters thick, these buoyant surface features are some of the most influential hydrological processes affecting ecosystem structure and

*Corresponding author: kelia.axler@noaa.gov

[§] Advance View was available online August 6, 2020

function in coastal, river-dominated regions around the world. River plumes have a characteristic hydrographic structure that results from the seaward projection of a turbid, low-salinity water mass. As buoyant plume waters move offshore, they overlay the higher salinity (denser) coastal shelf waters and are frequently accompanied by a variety of turbulent mixing processes as surface plume and shelf waters converge at the plume front (Garvine & Monk 1974). Buoyant and surface-seeking planktonic organisms can be swept up and passively carried by these converging water masses (Bowman & Iverson 1978, Olson & Backus 1985, Le Fèvre 1987), resulting in both retention and transport mechanisms that aggregate particulates, including zooplankton and ichthyoplankton, in high concentrations near the surface of the plume front (e.g. Govoni & Grimes 1992, Morgan et al. 2005, Peterson & Peterson 2008). In this way, river plumes structure larval fish distributions over both horizontal (cross-shore) and vertical (depth) spatial scales (Govoni 1997, Grimes 2001, Carassou et al. 2012).

Throughout their pelagic life, fish larvae must balance foraging for prey (e.g. copepods) with avoiding predators (e.g. gelatinous zooplankton; Houde 2002), and thus the degree to which river plumes spatially structure the nearshore plankton community has several important implications for larval fish population dynamics. As freshwater river plumes move through a coastal ecosystem, food availability and predator abundance often vary substantially on temporal scales commensurate with larval fish feeding, growth, and development. For example, if freshwater input into a nearshore system results in dense aggregations of zooplankton, these coastal environments should provide a recurrent, rich food resource that supports faster growth and higher survival of fish larvae. Therefore, via aggregation and retention of larval fishes and zooplankton, the timing and location of plume fronts may greatly impact nearshore fish populations, yet the direct effects of freshwater discharge on fisheries recruitment are neither clear nor consistent.

River plumes have been linked to higher larval fish survival in some fisheries (e.g. Grimes & Lang 1992, Lang et al. 1994, Rissik & Suthers 1996), but not others (e.g. Govoni & Chester 1990, Powell et al. 1990), suggesting that their effects can vary by species, freshwater source, and region. These inconsistencies could also be due in part to the fact that the same physical processes that concentrate fish larvae and their zooplankton prey within near-surface frontal zones can also increase encounter rates with known larval fish predators, such as gelatinous zooplankton

(e.g. ctenophores, hydromedusae, and siphonophores; Purcell & Arai 2001). These buoyant organisms have been found to aggregate across frontal boundaries in a variety of systems (Graham et al. 2001, McClatchie et al. 2012, Luo et al. 2014), potentially increasing mortality rates of plume-associated fish larvae. However, the turbid plume environment may also serve as a refuge if visual predators are unable to find fish larvae (Reichert et al. 2010), though it is unclear if this applies to tactile (non-visual) predators (i.e. gelatinous zooplankton). The highly dynamic nature of river plumes may also increase larval fish mortality. Periods of increased inland precipitation that result in prolonged coastal flooding events and high freshwater discharge into the nearshore region could result in an expansive plume that might transport larvae farther offshore and away from highly productive estuarine nurseries (Hjort 1926, Govoni 1997). In short, while it is well understood that river plumes play a prominent role in driving variability in coastal fisheries production and recruitment (Grimes 2001), the mechanisms behind this variability remain poorly resolved.

Advancing our understanding of the relationship between freshwater discharge and larval fish survival requires an approach that can repetitively quantify fine-scale *in situ* distributions of larval fish and their prey and predators over highly dynamic, large-scale features. Due to the influence of tides, winds, and volume of freshwater from upstream sources, river plumes frequently flood, ebb, meander, and dissipate on hourly, daily, and seasonal time scales (Stumpf et al. 1993, Govoni 1997). It is therefore necessary to examine distributions together with *in situ* hydrodynamic conditions over different 'plume regimes' (i.e. volume of freshwater discharge emitted and modifications to the structure of the plume itself due to tidal cycles, regional circulation patterns, and wind conditions). Recent developments in plankton imaging technology and machine learning techniques have made this comprehensive approach more feasible.

The northern Gulf of Mexico (nGOM) is a river-dominated region that drains the entire Mississippi River watershed yet also receives freshwater input from multiple other sources. Large sediment and nutrient loadings from both the Mississippi River and Mobile Bay system drive high primary and secondary productivity in the region, especially within plume frontal waters (Turner & Rabalais 1991, Cowan et al. 1996, Lohrenz et al. 1997). In the eastern Mississippi Bight, large volumes of brackish river/estuarine water exit through the narrow and shallow passes of Mobile Bay, regularly emitting large seasonal plumes onto

the Alabama continental shelf (Dinnel et al. 1990, Dzwonkowski et al. 2015). This inner shelf region immediately south of Mobile Bay supports a highly diverse larval fish assemblage and serves as an important nursery area for nearshore and estuarine-dependent fishes (Hernandez et al. 2010a,b). In addition, the generally well-described hydrographic conditions and shelf circulation of the region (Schroeder & Lysinger 1979, Dzwonkowski et al. 2011, 2014, 2015), make the Mobile Bay outflow a prime location to investigate fundamental questions regarding the effect of river plumes on larval fish ecology.

To examine how river plumes and their associated fronts affect the fine-scale distributions of larval fishes and their potential zooplankton prey and predators, we conducted an integrated physical and biological study near the Mobile Bay plume front. We contrasted the physical and biological characteristics of 3 distinct sets of physical conditions or ‘plume regimes’ throughout a peak Mobile Bay flood event: (1) a stratified water column with a shallow, low-salinity plume overlying saline coastal shelf waters in low wind conditions; (2) a deeper, slightly more mixed plume; and (3) a deep, well-mixed and highly turbulent plume water mass after the surface freshwater lens was mostly mixed away by strong winds. We describe and compare the physical structure of these habitats, and test for differences among them in the abundances and spatial relationships of larval fishes and their planktonic prey and predators.

2. MATERIALS AND METHODS

2.1. Study region

Mobile Bay is a wide yet shallow estuary in the nGOM that receives freshwater from the combined discharge of the Alabama and Tombigbee Rivers. The estuarine outflow of Mobile Bay has a long-term (1976–2011) daily mean discharge of $2656 \text{ m}^3 \text{ s}^{-1}$ during the spring season that forms a sizable plume (Dzwonkowski et al. 2014). While the extent of the plume varies in response to this flow (Dinnel et al. 1990), Mobile Bay discharges enough brackish water to produce a buoyant, turbid plume that extends tens of kilometers onto the continental shelf for much of the year (Schroeder & Lysinger 1979), with large plumes occurring when river discharge exceeds $4500 \text{ m}^3 \text{ s}^{-1}$ (Dinnel et al. 1990). For example, Dzwonkowski et al. (2015) observed an $\sim 8000 \text{ m}^3 \text{ s}^{-1}$ discharge event that created a plume extending ~ 60 km offshore of the

mouth of Mobile Bay. The dual outlet geomorphology of Mobile Bay (i.e. Main Pass to the south and Pass aux Herons to the west) creates a complex and highly variable bay/sound/shelf exchange, but modeling work by Kim & Park (2012) indicated that on average, 64% of the river water passes through a tidal inlet (Main Pass) into the Gulf of Mexico, while Pass aux Herons transmits the remainder westward to the Mississippi Sound. Like most of the estuaries in this region, the bay has a small diurnal tide (~ 0.5 m range at Dauphin Island) that causes the plume to pulse onto the shelf with ebb currents (Gelfenbaum & Stumpf 1993). Water column structure (e.g. stratification and mixing) on the shelf is largely driven by wind stress and river discharge (Dzwonkowski et al. 2018a,b). Given the shallow depth of the Alabama shelf region, wind stress can stimulate a nearly complete mixing of the water column and a downward advection of surface waters, resulting in weak, if any, stratification. However, at other times (e.g. during light wind conditions) the water column may be highly stratified, leading to well-defined density fronts along the plume boundaries that increase the complexity of their interaction with shelf waters (Gelfenbaum & Stumpf 1993).

2.2. River plume sampling

To examine the influence of river plumes on the spatial distributions of larval fishes and zooplankton and as part of a larger field campaign for the interdisciplinary Consortium for oil exposure pathways in Coastal River-Dominated Ecosystems (CONCORDE) program (see Greer et al. 2018), we collected both *in situ* plankton imagery and biological samples during a 2 wk cruise in the Mississippi Bight aboard the RV ‘Point Sur’ from 30 March to 11 April 2016. Larval fishes and zooplankton were sampled across multiple freshwater pulses exiting the mouth of Mobile Bay by towing the high-resolution *In Situ* Ichthyoplankton Imaging System (ISIIS; Cowen & Guigand 2008) throughout the largest freshwater discharge event of 2016. The ISIIS was towed behind the RV ‘Point Sur’ to sample a transect approximately 20 km in length that arced from east to west around the mouth of Mobile Bay. The transect extended $\sim 10\text{--}15$ km due south of Main Pass at its apex and $\sim 5\text{--}10$ km offshore on either end in depths between 10 and 20 m (Fig. 1A). All 3 transects were similar in length and sampled inside of the 20 m isobath. The transect was sampled 3 times: during daylight hours between $\sim 10:00$ and $14:00$ h CDT on 9 April and between

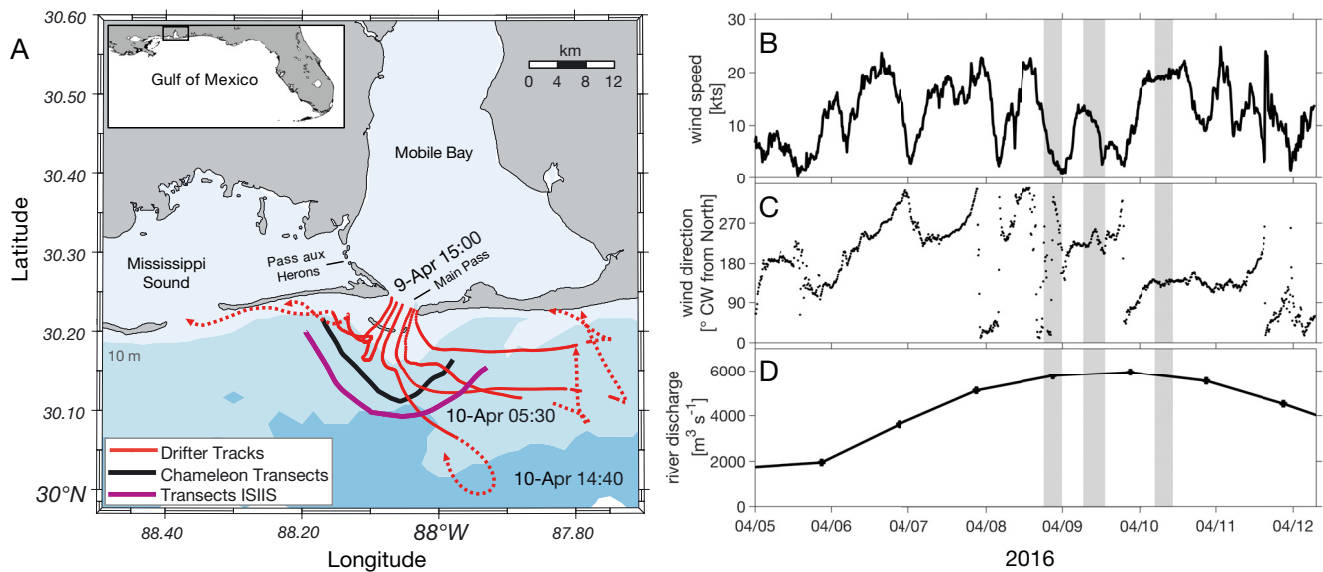


Fig. 1. (A) Study area at the mouth of Mobile Bay (Alabama, USA). On 9–11 April 2016, the plankton imager (*In Situ* Ichthyoplankton Imaging System, ISIIS) was towed 3 times in a 20 km long arc (purple line) through the Mobile Bay plume outflow to sample the *in situ* distributions of larval fishes and zooplankton. The Chameleon microstructure profiler was towed ~3 km inshore (black line) over the same time period to characterize the physical properties of each plume. Six surface-configured (top 1 m) drifters were deployed from Main Pass at 15:00 h on 9 April 2016 to track the advection of a plume on an ebb tide in low wind conditions (solid red lines) and during strong southeasterly winds (dotted red lines). (B) Wind speed (knots), (C) wind direction (° clockwise [CW] from north), and (D) river discharge ($\text{m}^3 \text{s}^{-1}$) from Mobile Bay are shown using a lag time (6 d) for the inland measured volume. Grey shaded regions indicate sampling periods during the ISIIS and Chameleon transects. Wind data were averaged into 10 min bins, and the wind direction is the direction that the wind was coming from

~21:00 and 02:00 h CDT on the nights of 9–10 and 10–11 April 2016.

Images of fish larvae and zooplankton (Fig. 2) were captured using the ISIIS, a towed shadowgraph imager that uses a line-scan camera to sample large volumes of water ($150\text{--}185 \text{ l s}^{-1}$; Cowen et al. 2013). The ISIIS undulates from within ~1 m of the surface to within 2 m of the bottom using motor-actuated wings at a horizontal speed through the water of $\sim 2.5 \text{ m s}^{-1}$ and vertical speed of $0.2\text{--}0.3 \text{ m s}^{-1}$. Two cameras imaged zooplankton between approximately 500 μm and 12 cm in length while simultaneously measuring salinity, temperature, and depth (Sea-Bird Electronics 49 FastCAT), dissolved oxygen (SBE 43), chl a fluorescence (Wet Labs FLRT), and photosynthetically active radiation (PAR; Biospherical QCP-2300). The images and oceanographic data are linked by a common timestamp, which enables a detailed description of the physical environment for each individual organism. Full water column profiles were used to quantify changes in the vertical and horizontal structure of planktonic distributions, enabling a fine-scale examination of larval fish distributions and associated predator and prey fields across each plume regime. A Bedford Institute of Oceanography Net Environmental Sampling System (BIONESS; Open Seas Instrumen-

tation) was also towed within Mobile Bay plume waters and shelf (non-plume) waters to capture larval fishes and zooplankton that were used to verify ISIIS image classifications and develop the ISIIS image library (see Section 2.5).

2.3. River plume physical characterization

At the same time ISIIS measured the distribution of planktonic organisms along a transect around the Mobile Bay outflow, a second vessel (the RV 'Pelican') sampled a parallel transect ~3 km upstream and north of the ISIIS transect (Fig. 1A), measuring profiles of microstructure turbulence, temperature, conductivity, optical backscatter (800 nm), and fluorescence using the Chameleon microstructure profiler (Moum et al. 1995). River plumes were identified by their unique physiochemical signatures using a combination of surface-configured (top 1 m) CODE/DAVIS-style drifting buoys (hereafter referred to as 'drifters'), ISIIS-mounted environmental sensors (Sea-Bird SBE 49 FastCAT, Sea-Bird 43, Wet Labs FLRT, and Biospherical QCP-2300), hull-mounted shipboard acoustic Doppler current profilers (Teledyne RD Instruments; 300 and 1200 kHz RDI Work-

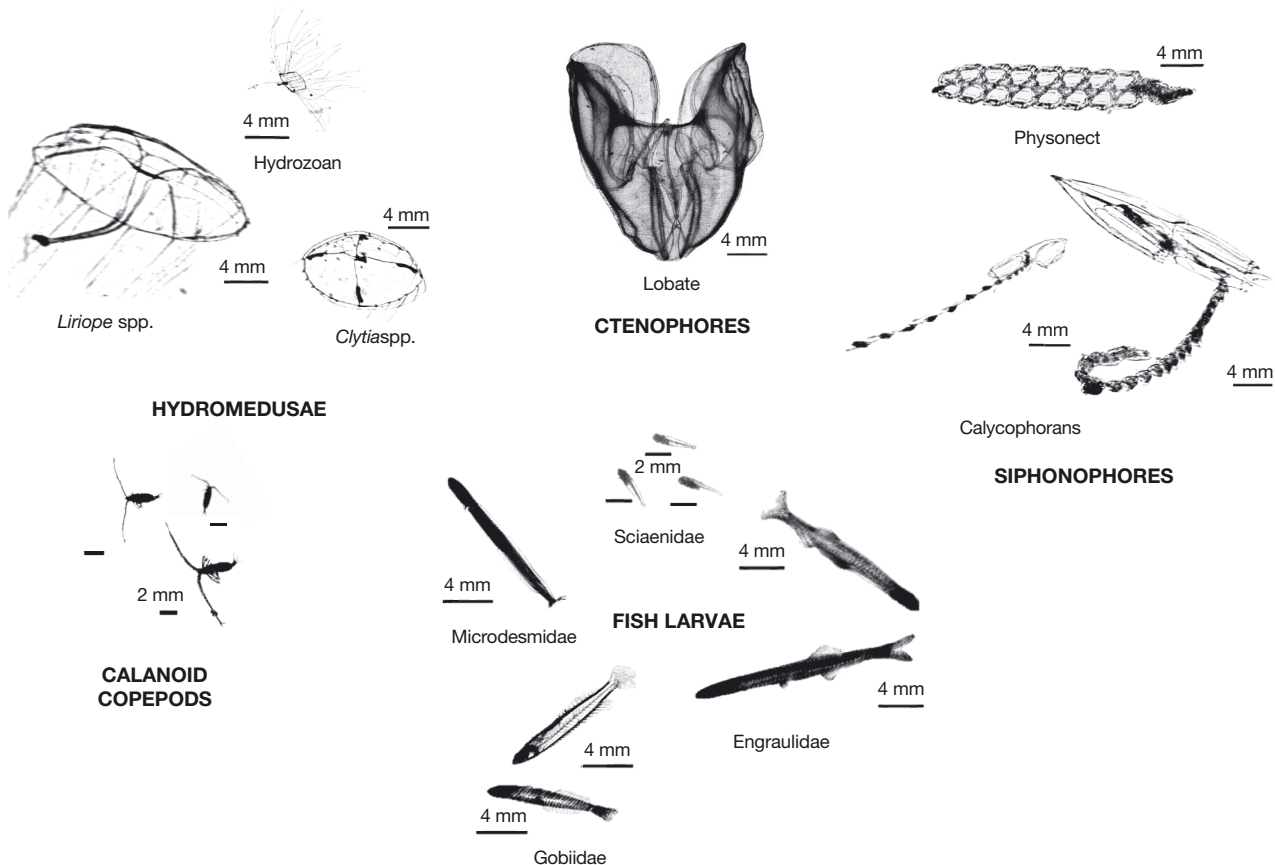


Fig. 2. Example shadowgraph images of fish larvae, calanoid copepods, ctenophores, hydromedusae, and siphonophores captured by the ISIIS in the Mobile Bay plume outflow on 9–11 April 2016. Scale bars are given for each individual

horse, depending on depth), and the Chameleon microstructure profiler. All Chameleon measurements extended from the surface to within 2 cm of the bottom, except turbulence, which was contaminated by instrument vibration in the upper 4 m. Because of this, it is important to note that the turbulence values within the plume (upper water column) were likely higher than reported here. Dissipation was calculated from the Chameleon microstructure measurements as per Moum et al. (1995). The total turbulent kinetic energy dissipation rate (W kg^{-1}) for each transect was calculated by averaging the dissipation over all depths from 5 m below the surface (the shallowest turbulence bin) to within 1 cm of the bottom. The magnitude of turbulence within each water mass was calculated by averaging above (plume dissipation) and below (shelf dissipation) the halocline (salinity of ~34; the approximate isocline that delineated plume from shelf water masses). Average wind speed and direction were collected from anemometers on the RV 'Pelican.' From this suite of oceanographic data, we were able to delineate the geographic position, movement, depth, and boundaries of the Mobile Bay plume for each day of sampling, yielding a detailed

view of estuarine-shelf processes and corresponding oceanographic and biological responses.

2.4. Mean river discharge

River discharge data were obtained from 2 USGS gauging stations, the Claiborne Lock & Dam on the Alabama River (USGS 2016a) and the Coffeeville Lock & Dam on the Tombigbee River (USGS 2016b), both of which are approximately 238 km upstream of the mouth of Mobile Bay. These stations are typically used to compute the river discharge volume that contributes to brackish water exiting the bay in a plume. Their summed discharge was extrapolated for the entire delta watershed (Q_2) following the method of Schroeder (1979):

$$Q_2 = \frac{A_2}{A_1} \times Q_1 \quad (1)$$

where Q_1 is the summed discharge, A_1 is the station watershed area, and A_2 is the delta watershed area (Fig. 1D). To identify the time of peak river discharge, measurements were lagged 6 d to account for travel time from the upriver gauging stations to the mouth

of the bay (Dinnel et al. 1990, Dykstra & Dzwonkowski 2020).

2.5. Plankton image processing and automated classification pipeline

A sparse convolutional neural network (sCNN) was used to automate identification of ISIIS-imaged taxa following the image processing pipeline model of Luo et al. (2018). Here we present a summary of the pipeline, which included 4 major steps: (1) background correction and image segmentation; (2) automated classification using an sCNN and a training library specifically built for the Mississippi Bight; (3) quality analysis and control (e.g. removing classified data with low-probability values) and confusion matrix analyses (to obtain correction factors); and (4) application of correction factors to the final abundance estimates used in this work.

All collected ISIIS images were segmented into single frames and the frames were automatically processed using a 'flat-fielding' technique that removed image background. Regions of interest (e.g. single planktonic organisms; hereafter referred to as 'vignettes') were then extracted and saved in preparation for the automated classification pipeline. The 'SparseConvNets with Fractional Max-Pooling' (Graham 2015) configuration was used to train the sCNN until an error rate of $\leq 5\%$ was achieved as per Luo et al. (2018). The sCNN was trained and tested by randomly extracting and manually identifying 45 594 vignettes originating from CONCORDE transects spanning 3 surveys across 3 seasons to capture the diversity of organisms (and image quality due to variable, but high turbidity) in a variety of water conditions (Fig. 2). The training library was composed of 173 unique classes that included biological taxa, particles, and noise due to Schlieren effects and bubbles at the surface or at sharp density discontinuities.

The sCNN assigned the probability that each image belonged to any of the 173 taxon classes; however, each vignette was assigned to the class with the highest probability. A loess model was used to determine at which probability threshold a cutoff should be made to reach 90% classification precision (Luo et al. 2018). The model used an independent test set of 15 199 vignettes whose automated classifications were manually corroborated. This probability filtering was then applied to remove images whose probabilities fell below that threshold, which still allowed for the prediction of true spatial distributions (Faillettaz et al. 2016). At the same time that vignettes were threshold

filtered, classes were re-grouped. This regrouping was justified because a single taxon was oftentimes represented by different classes, each comprised of body orientations/postures, life stages, and sex. Thus, for the final analyses, after classification and thresholding, the original 173 classes were condensed into 89 groups.

To evaluate the final automated classification pipeline performance, a confusion matrix was generated for another independent set of 91 984 randomly selected classified vignettes. After the filtering thresholds were applied and classes were mapped out into final groups, F_1 -scores (harmonic mean of precision and recall, $F_1 = 2 \times P \times R/[P + R]$) were calculated using the number of true positives (TP), false positives (FP), false negatives (FN), precision ($P = TP/[TP + FP]$), and recall ($R = TP/[TP + FN]$).

Timestamps were then used to merge the classified imagery data with the environmental data (salinity, temperature, depth, fluorescence intensity, dissolved oxygen, and photosynthetically active radiation [PAR]) collected by ISIIS, and these were binned into 1 m vertical strata along the sampling path through the water. The resulting data were then used to estimate concentrations of organisms (ind. m^{-3}) based on the volume of water imaged, calculated average tow speed, and time spent by ISIIS in each 1 m vertical stratum. Finally, a correction factor (*sensu* Hu & Davis 2006) based on the results of the final confusion matrix was applied to the concentrations of each group (i.e. taxon) using the following equation:

$$\text{Correction factor (taxon)} = \frac{\text{Precision rate (taxon)}}{\text{Recall rate (taxon)}} \quad (2)$$

Although there were 89 different groups of plankton taxa in the CONCORDE data, and 693 million vignettes were identified in an automated fashion from the 3 plume transects in our field sampling, only key taxa that were deemed to be ecologically important prey or predators of larval fishes were used in this study (Fig. 2). Furthermore, plankton data were combined into higher taxonomic categories for ease of analysis and to better enable the comparison of fish larvae with their prey and predator groups. The resulting categories were: the prey category 'Calanoid copepods' (comprised of original groups *Acartia* spp., *Centropages* spp., Paracalanidae, and unidentified calanoid copepods informally called 'small and stubby'), and the predator categories 'Ctenophores' (lobate and cydippid ctenophore classes combined), 'Hydromedusae' (comprised of *Liriope* spp., *Clytia* spp., *Mnemiopsis* spp., *Corymorphida* spp., and the Hydrozoa *Solmaris* spp.), and siphonophores (*Muggiaeae* spp., *Sphaeronectes* spp., and various physonects).

Calanoid copepods were chosen to represent the larval fish 'prey' category because they are a rather ubiquitous prey group for many fish larvae in this region (McNeil & Grimes 1995, Holt & Holt 2000), including for 2 dominant species. We conducted a diet study on net-captured fish larvae from stations in the immediate vicinity of the ISIIS transects during the same sampling period (8–11 April 2016). Engraulidae and Sciaenidae were the 2 most abundant larval fish taxa in both the ISIIS images and the nets, and gut content analyses on the 2 most common species within each family, striped anchovy *Anchoa hepsetus* (Engraulidae; $n = 166$) and sand seatrout *Cynoscion arenarius* (Sciaenidae; $n = 172$), confirmed that calanoid copepods were major prey items (Axler 2019). Similarly, ctenophores, hydromedusae, and siphonophores are known to be voracious predators of fish larvae (Purcell & Arai 2001) and were therefore selected to represent the 'predator' categories.

Images of larval fishes from each transect were extracted by the sCNN using the same automated methodology as the zooplankton imagery. However, since these were rare organisms and their numbers in the training data set classes were unbalanced with respect to the more abundant groups, automated classified larval fish images were manually reviewed by a human expert to verify correct identifications and to achieve lower taxonomic classifications than the sCNN was trained to do. This might have left the false negative fish larvae unaccounted for; however, fishing manually for these false negatives would have been nearly impossible given the large number of images in this imagery data set.

2.6. Statistical analysis

To compare distributions of fish larvae and zooplankton across plume regimes, taxa concentrations (ind. m^{-3}) were calculated by using the volume of water imaged, average tow speed, and time spent in each 1 m vertical bin. The length of each horizontal bin was roughly similar but varied slightly ($<10s\ m$) depending on the tow speed of the ISIIS vehicle and time spent in each 1 m vertical stratum. The samples used for analysis were the concentrations of different taxa in each 1 m vertical depth bin. The samples in the stratified transect ($n = 1918$), slightly-mixed transect ($n = 2064$), and well-mixed transect ($n = 2172$) were summed over each transect, and a Kruskal-Wallis test was applied to compare concentrations among the 3 transects for all individual categories of taxa (fish larvae, calanoid copepods, ctenophores,

hydromedusae, and siphonophores). Normality of distributions and homoscedasticity of variances were evaluated by examining diagnostic plots of residuals in R. Histograms and residual quantile-quantile plots showed that the concentrations of each taxon among all transects were highly non-normal. Log($x + 1$)-transformations of the concentration data improved the spread of the residuals across the fitted values and resulted in relatively homogeneous variance among the 3 transects. However, the transformations did not result in normal distributions of the data, so concentrations were compared using nonparametric Kruskal-Wallis tests and post hoc Dunn's tests for pairwise comparisons using the 'FSA' package (Ogle et al. 2020) in R (v4.3.1; R Core Team 2019).

Weighted mean depths (WMDs) of larval fishes, calanoid copepods, ctenophores, hydromedusae, and siphonophores were calculated to assess differences in the vertical distributions of taxa over time and by plume regime following the methods of Frost & Bollens (1992):

$$WMD = \frac{\sum(n_i \times d_i)}{\sum n_i} \quad (3)$$

where n_i is the concentration of individuals per cubic meter of taxon i at depth d , which is taken to be the shallowest point of each 1 m depth stratum.

Concentrations (ind. m^{-3}) of 1 m vertically binned organisms were also used to assess the fine-scale correlations between fish larvae, prey, and predator taxa, as well as to determine whether high abundances of organisms were correlated with different environmental variables (temperature, salinity, oxygen, fluorescence) across plume regimes using non-parametric Spearman rank correlation coefficients. The significance levels of the correlation coefficients were determined using an approximation of the Student's t distribution in the 'Hmisc' package in R (Harrell 2019), with a conservative p-value significance threshold of 0.01. Data visualization was performed in R (R Core Team 2019) using the packages 'dplyr' (Wickham et al. 2018) and 'ggplot2' (Wickham 2016) and in MATLAB (MathWorks' MATLAB, version R2018b).

3. RESULTS

3.1. Environmental and physical oceanographic setting

In mid-April 2016 under high river discharge conditions, Mobile Bay emitted a brackish plume into the nGOM coastal waters, but its position and physi-

cal structure were modified greatly by wind-forcing and ambient circulation. We sampled 3 distinct plume regimes (transects) that varied by degree of wind-forcing, turbulence, and resulting water column mixing: on 9 April we sampled a highly stratified water column with a shallow plume in low wind conditions, on 9–10 April, a deeper, slightly-mixed plume, and on 10–11 April, a deep, well-mixed and highly turbulent plume water mass under high wind stress.

Average river discharge ($\leq 2000 \text{ m}^3 \text{s}^{-1}$) and light westerly winds (≤ 9 knots on average) prevailed the week preceding our sampling efforts. On 7–8 April, river discharge increased to nearly $5000 \text{ m}^3 \text{s}^{-1}$, and winds were highly variable though primarily from the west (Fig. 1B–D), setting up a stratified water column with a shallow lens of turbid, low-salinity plume water overlying the clearer, higher-salinity shelf water for our first day of sampling. On 9 April, upwelling conditions (westerly winds) forced the plume offshore (south) where it was advected eastward by shelf currents (Fig. 3A,D). The plume-tracking drifters, released on 9 April 2016 at ~15:00 h from the eastern and central side of Main Pass, verified these observations by moving offshore and to the east (Fig. 1A). In contrast, drifters released on the west side of Main Pass were retained for nearly 7 h in a localized region ~5 km south of Dauphin Island and 10–15 km west of Main Pass, likely due to the strong hydrodynamic convergence associated with eastward wind-driven currents on the shelf arresting the westward expansion of the surface-adverted tidal plume exiting Mobile Bay. During these low wind conditions, the turbulent kinetic energy dissipation rate (ϵ) was $1.2 \times 10^{-6} \text{ W kg}^{-1}$ averaged over the entire water column, $2.7 \times 10^{-6} \text{ W kg}^{-1}$ averaged within and slightly below the plume (water with salinity approximately 34 or less), and $6.6 \times 10^{-7} \text{ W kg}^{-1}$ averaged in the underlying shelf waters (Fig. 4A). The near-surface plume was observed in the middle portion of our transect with an east–southeastward velocity of $\sim 0.3 \text{ m s}^{-1}$, while some shoreward (northward) advection of near-bottom water was observed below the plume (Fig. 3D). Light winds and a shallow (~3 m thick), low-salinity plume created a distinct halocline with a salinity difference > 15 that separated the relatively fresh and turbid water of the plume from the saltier, clearer water below (Fig. 4A). Strong stratification between layers limited the vertical exchange of suspended sediments and chlorophyll *a* (as observed in the fluorescence plots, Fig. 4A).

Overnight on 9–10 April, winds switched from light and variable to light and predominately southwestward, with winds averaging 6.9 knots (Fig. 1B,C). The switch trapped the western portion of the plume

against the shallow mouth bar, causing the halocline and chlorophyll layer to deepen to ~8 m and producing a much thicker plume than was observed in the first transect (Fig. 4B). The plume in the eastern portion of the transect continued advecting southeastward by strong near-surface currents (Fig. 3E; $\geq 0.5 \text{ m s}^{-1}$) and an ebbing tide. Turbulence dissipation increased with the higher river input to $2.1 \times 10^{-6} \text{ W kg}^{-1}$ averaged over the entire water column and $4.2 \times 10^{-6} \text{ W kg}^{-1}$ averaged in the plume, and decreased slightly in the underlying shelf waters to $5.7 \times 10^{-7} \text{ W kg}^{-1}$, which continued their slow (~ 0.1 – 0.2 m s^{-1}) shoreward movement (Fig. 4B).

A very different regime of wind, stratification, and mixing was observed the night of 10–11 April (Fig. 3C). The wind shifted direction and began blowing strongly from the east–southeast, building to nearly 20 knots (Fig. 1B,C). This advected the surface waters inshore against the Alabama coastline as evidenced by the reversal in direction of the drifters at ~10:00 h (Fig. 1A). At the same time, the deeper ambient shelf currents switched to the southwest in response to the wind forcing and traveled seaward at $\sim 0.3 \text{ m s}^{-1}$ (Fig. 3F). Further, the change in wind direction, shifting from upwelling favorable to downwelling favorable, likely dissipated (or at least reduced the intensity of) the region of convergence on the western end of the transect, releasing the 2 stalled drifters and allowing them to enter a westward-directed buoyant coastal current on the following ebb tidal plume that ultimately pulled them into the Mississippi Sound (Fig. 1A). These intense downwelling conditions eroded the stratification and homogenized the upper 10 m of the water column to a near-uniform salinity of 25 (Fig. 4C; the exception being a 5 m deep, 2 km wide eddy with salinity of 20 that was observed by RV 'Pelican' at 88.1°W). Meanwhile, the Mobile Bay outflow reached the highest discharge of the entire year of $\sim 5944 \text{ m}^3 \text{s}^{-1}$ on 10 April (Fig. 1D). Turbulence dissipation rates increased 3-fold from the first transect to $3.7 \times 10^{-6} \text{ W kg}^{-1}$ averaged over the entire water column. Average dissipation was $4.2 \times 10^{-6} \text{ W kg}^{-1}$ within the plume and $8.9 \times 10^{-7} \text{ W kg}^{-1}$ in the underlying shelf water. Note that the plume shifted even farther east, so the strongest turbulence and eastward currents were observed on the eastern half of the transect, and within the eddy at 88.1°W (Fig. 4C). In summary, buoyant plume waters were characterized by both stronger currents and higher turbulence than the underlying and adjacent shelf waters. There was also a trend of heightened current velocity and turbulence over the study period as wind speeds increased.

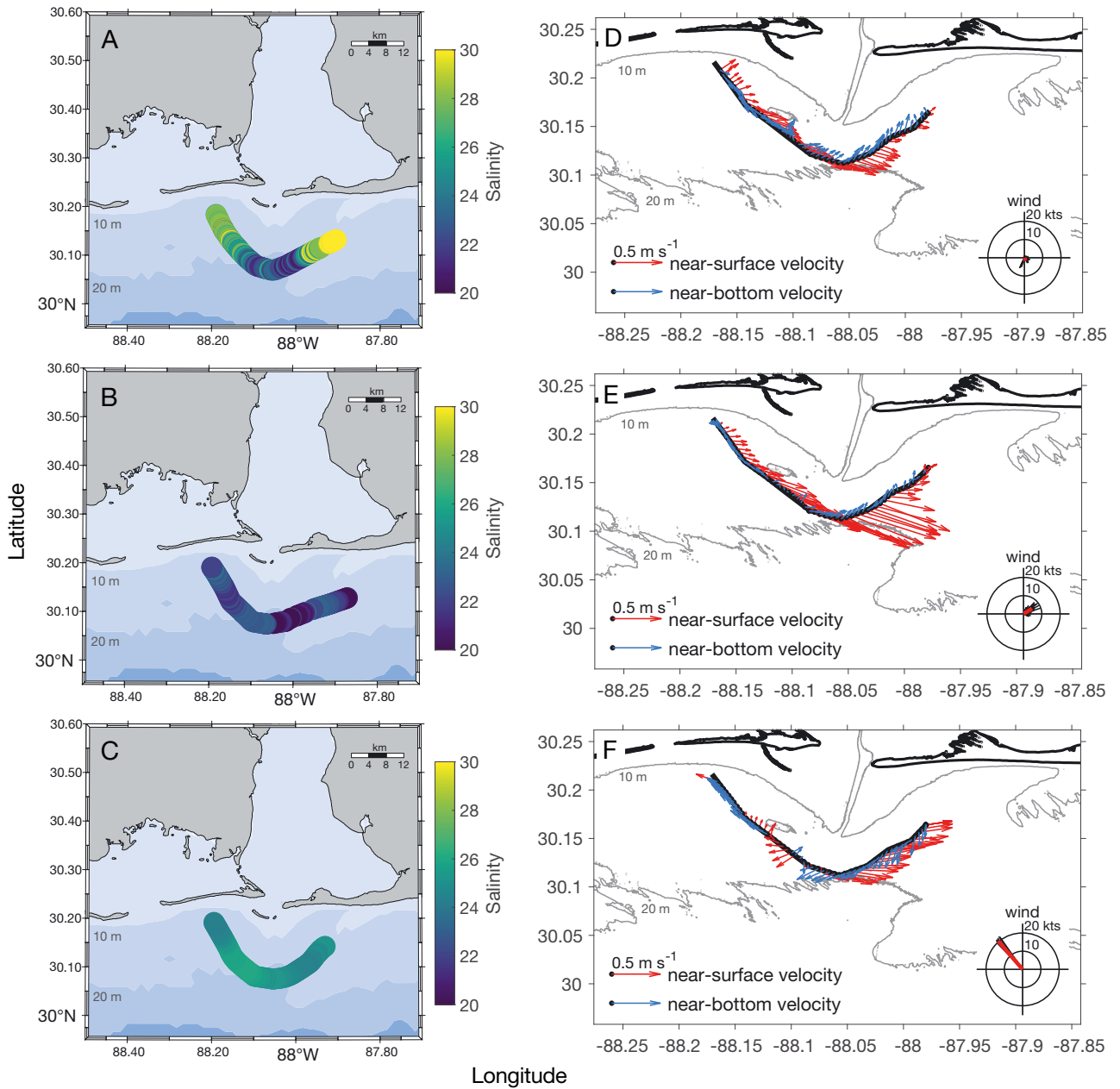


Fig. 3. (A–C) Series of near-surface (<2 m) salinity values measured by the arcing tows of the ISIIS around the mouth of Mobile Bay show the stratified (A), slightly-mixed (B), and well-mixed (C) plume regimes sampled during the large discharge event in April 2016. (D–F) Near-surface (3.5 m; red arrows) and near-bottom (within 2–4 m of bottom; blue arrows) current velocities as measured by a shipboard acoustic Doppler current profiler are plotted along the transect path. Insets show average wind direction and speed (plotted in the oceanographic convention to be in the same coordinate system as the current velocities) during each sampling event. Wind plots show 10 min averaged wind vectors in black and an average over the entire transect in red

3.2. Fine-scale vertical and horizontal distributions of key taxa across different plume regimes

Fish larvae and zooplankton exhibited large spatial and temporal variability in their overall abundances and vertical and horizontal distributions across the 3 different plume regimes. A total of 941 fish larvae

were manually verified from the automated classified images. The most abundant families were Engraulidae (28.7%), Sciaenidae (19.3%), Microdesmidae (12.0%), and Gobiidae (4.3%). Approximately 33% of larval fishes found were not identifiable to family level due to poor image quality, fish orientation into the camera, or a lack of visible meristics.

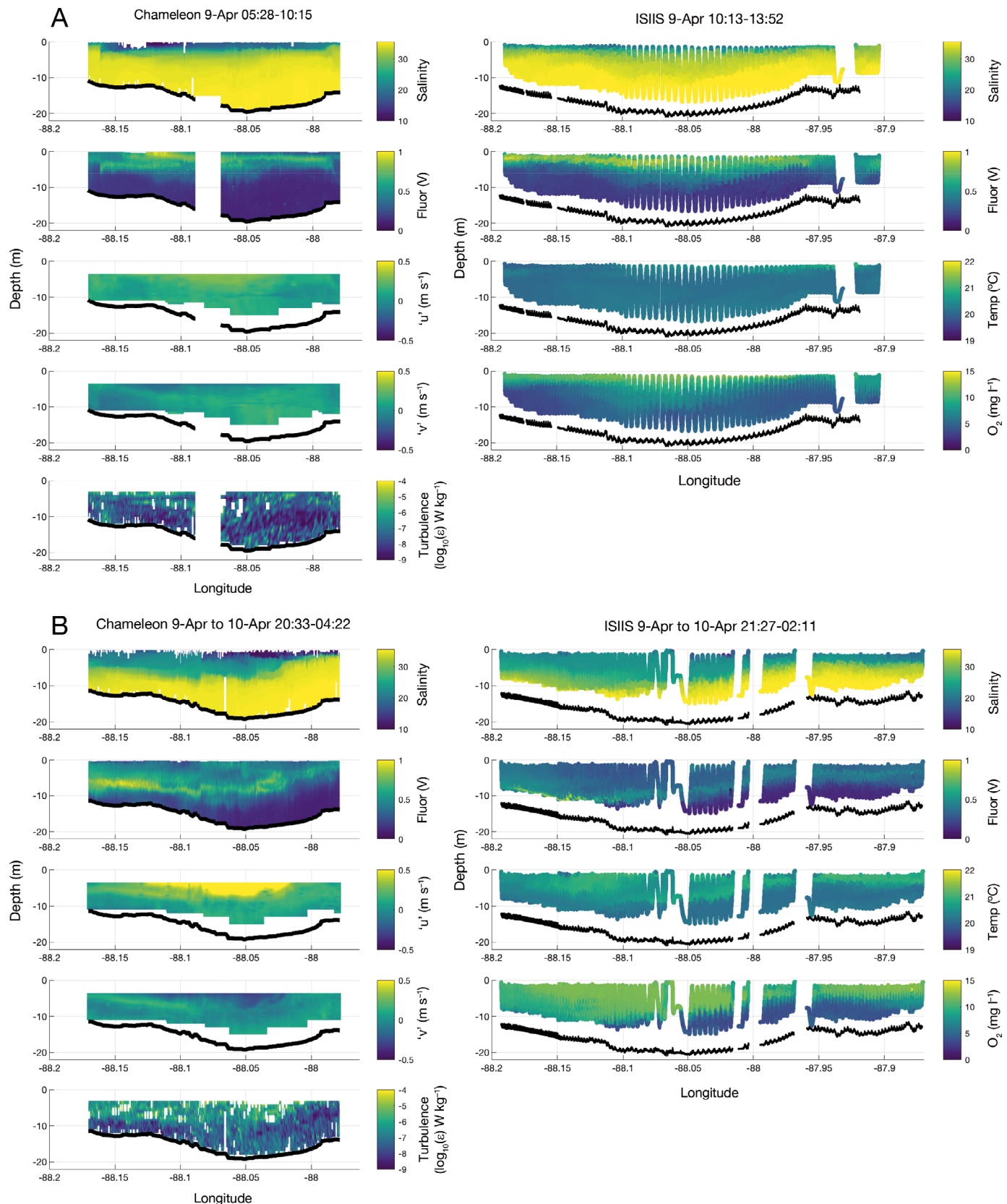


Fig. 4. Environmental data profiles of the Mobile Bay nearshore region during: (A) stratified (9 April), (B) slightly mixed (9–10 April), and (C) well-mixed (10–11 April) plume regimes from spatiotemporally similar Chameleon microstructure transects (left panels) and ISIIS transects (right panels). Black lines indicate bathymetry
(continued on next page)

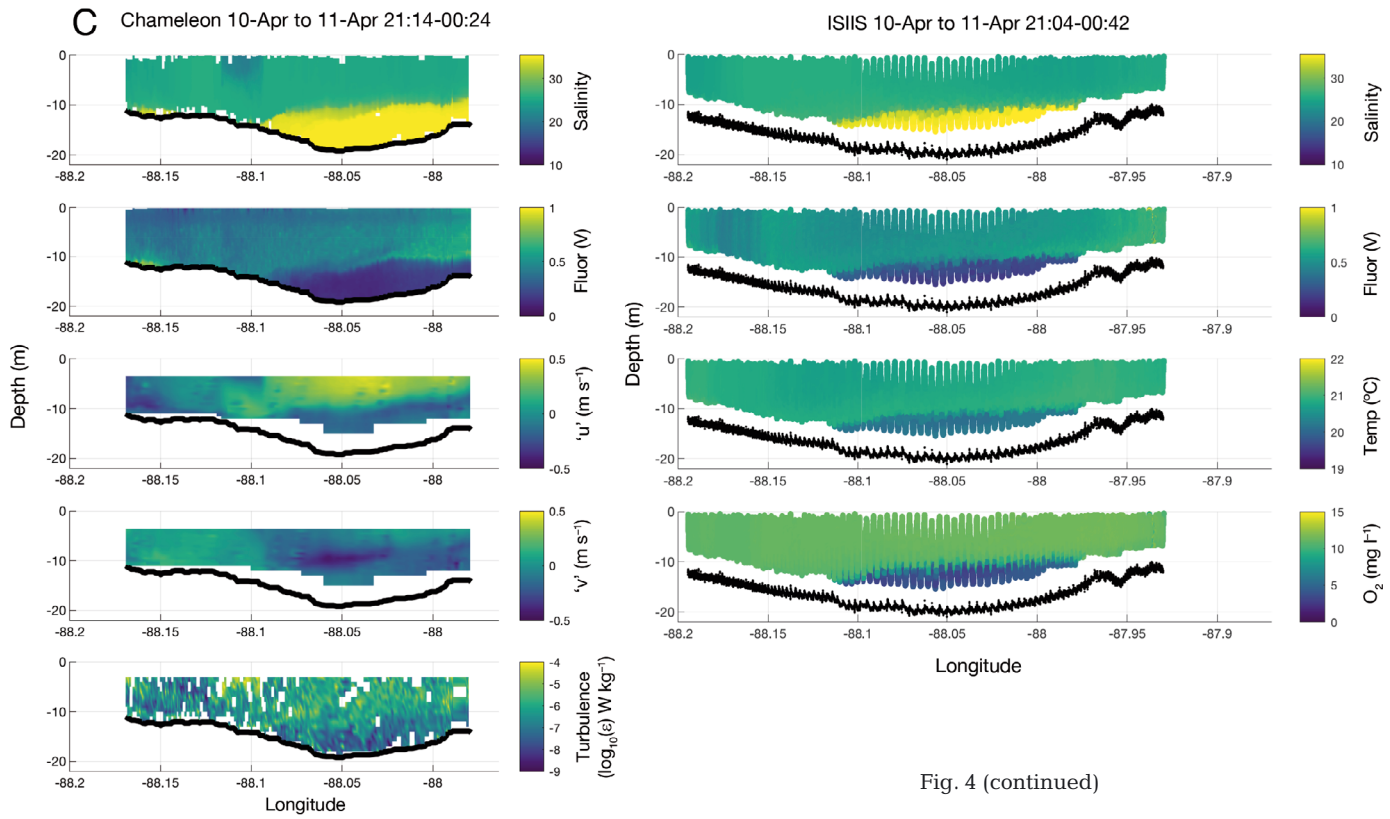


Fig. 4 (continued)

The abundance of larval fishes in the ISIIS images was highly variable across plume regimes: peak larval fish concentrations differed significantly among the 3 transects ($\log(x + 1)$ -transformed, Kruskal-Wallis: $H = 170.58$, $\text{df} = 2$, $p < 0.0001$). Zooplankton concentrations (ind. m^{-3}) also differed significantly across the 3 plume regimes for all taxa ($\log(x + 1)$ -transformed Kruskal-Wallis tests, $p < 0.05$ for all taxa comparisons; Fig. 5), beginning as a dense, multi-taxon aggregation in the upper 6 m of the water column during the stratified regime (Fig. 6A) and becoming increasingly dispersed, with most taxa decreasing in concentration over the study period as turbulence and advective processes strengthened over time (Fig. 5).

Biological aggregation occurred on the western end of the transect where drifters indicated elevated hydrodynamic convergence (Fig. 7A,D,G,J,M). Prevailing westerly winds and upwelling-favorable conditions during the week prior to sample collection suggests that this frontal convergence may have been present for at least a few days, aggregating plankton and creating a potentially rich feeding environment for fish larvae. The highest concentrations ($\pm \text{SE}$) of transect-averaged larval fishes ($0.321 \pm 0.014 \text{ ind. m}^{-3}$), calanoid copepods ($5.36 \pm 0.096 \text{ ind. m}^{-3}$), ctenophores ($0.283 \pm 0.012 \text{ ind. m}^{-3}$), and siphonophores ($1.86 \pm 0.042 \text{ ind. m}^{-3}$) occurred in

these low-wind, stratified conditions likely due to the dense accumulation of plankton in the convergent region. The WMD of fish larvae was 3.9 m, which was within 1.5 m of the WMD of both prey and predator taxa, all of which were distributed slightly more deeply than fish larvae (Fig. 6A). While most of the biomass was concentrated in the western end of the transect, fine-scale distributions of organisms varied greatly by distance along the transect. The middle portion of this transect, for example, was subjected to the direct eastward flow ($\sim 0.3 \text{ m s}^{-1}$) of the plume (Fig. 3D). As a result of this offshore advection, relatively few fish larvae and gelatinous zooplankton were observed in these regions (Fig. 7A,D,G,J,M). Calanoid copepods were densely clustered at both east and west ends of the transect, but less concentrated in the middle of the transect where the plume currents were strongest. Interestingly, fish larvae were found to co-occur with their copepod prey on the western end of the transect but not the eastern end, where a similar aggregation of calanoid copepods was recorded.

As the halocline deepened the following night of 9–10 April, fish larvae were distributed more deeply in the water column ($\sim 5.4 \text{ m}$) and at approximately the same WMD as calanoid copepods (5.0 m; Fig. 6B). Gelatinous zooplankton varied across this transect, with hydromedusae more deeply distributed (6.3 m)

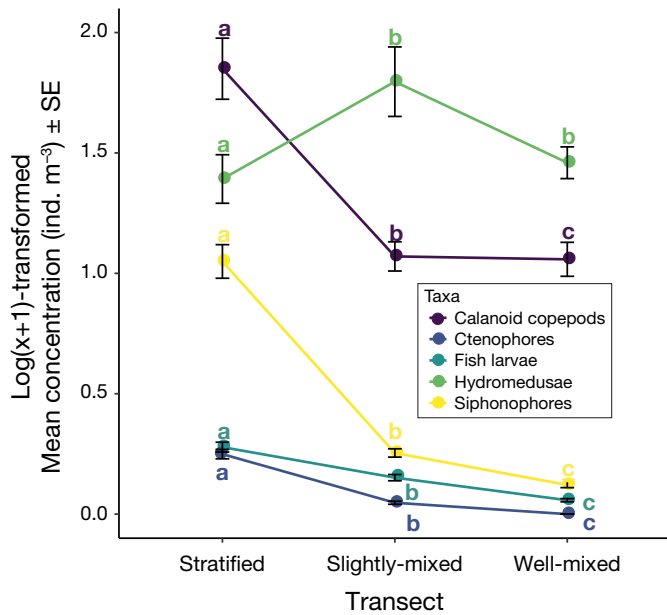


Fig. 5. $\text{Log}(x + 1)$ -transformed mean concentrations ($\pm \text{SE}$) of fish larvae and zooplankton taxa across the 3 plume regimes (transects). Results of Dunn's test post hoc pairwise comparisons are indicated by lowercase letters for comparisons of concentrations among plume regimes

while ctenophores and siphonophores were shallower than in the previous transect (3.6 and 4.6 m, respectively). As river discharge continued to increase and ebb tidal currents advected the plume offshore, all taxa decreased in overall abundance and became patchier in distribution (Fig. 7B,E,H,N) with the exception of hydromedusae, which became significantly more abundant (Fig. 5) and appeared to aggregate along the halocline (Fig. 7K). A patch of fish larvae remained concentrated on the western edge of the transect, suggesting that the region of convergence was still present, yet plume currents were strong enough to disperse most of the fish larvae and zooplankton eastward and offshore (Fig. 7B).

As the winds reversed and strengthened overnight on 10–11 April and mixing increased further, larval fishes and zooplankton became even less abundant overall (Fig. 5) and more dispersed in their fine-scale distributions (Fig. 7C,F,I,L,O), consistent with both horizontal advection by wind and tidal currents and vertical mixing. Fish larvae were even more deeply distributed (6.5 m WMD) than in the previous 2 transects and were on average 1.5 m deeper in the water column than their potential copepod prey, yet also 1.2 to 1.5 m deeper than the gelatinous taxa (hydromedusae and siphonophores; Fig. 6C). Ctenophores were entirely absent from the well-mixed plume regime. It seems likely that the region

of elevated convergence observed in the stratified transect is a regularly occurring feature as calanoid copepods and hydromedusae were detected re-aggregating within this same region during the next ebb tide (Fig. 7F,L).

3.3. Physical and biological correlations

Spearman correlation coefficients indicated that the fine-scale physical environment experienced by our focus plankton categories varied widely across the different plume regimes. In general, plume water was characterized by significantly lower salinity (≤ 25) yet higher fluorescence ($\geq 0.4 \text{ V}$) and oxygen ($\geq 9 \text{ mg l}^{-1}$) than the underlying shelf water, with increasing stratification in the water column (Fig. 4). Temperature varied little ($< 1^\circ\text{C}$) between the water masses, although Mobile Bay plume water was generally slightly warmer ($\geq 20.8^\circ\text{C}$ on average) than the underlying coastal shelf water ($\leq 20.3^\circ\text{C}$).

In low wind and stratified conditions (9 April), concentrations of fish larvae, calanoid copepods, ctenophores, hydromedusae, and siphonophores were significantly positively correlated with fluorescence and negatively correlated with salinity, reflecting their close association with the highly productive, low-salinity plume water masses (Fig. 8A). In the slightly mixed regime (9–10 April), stronger winds began eroding the stratification between water masses and resulted in weaker and more variable correlations between physical conditions and taxa concentrations (Fig. 8B). For example, fish larvae and siphonophores became less associated with the plume and not significantly correlated with any of the physical variables measured. Only copepods and ctenophores remained correlated with plume water masses. In the well-mixed regime (10–11 April), wind-induced downwelling largely homogenized the water column in the upper 10 m, although high-salinity (~35) shelf waters remained in the bottom 2–3 m. Fish larvae, calanoid copepods, and siphonophores had generally weak and variable relationships with all physical variables, likely indicative of their variable distributions throughout the highly mixed plume water mass characterized by moderate salinity (~25), oxygen ($10–11 \text{ mg l}^{-1}$), and fluorescence ($0.5–0.7 \text{ V}$; Fig. 8C). Hydromedusae, however, were slightly correlated with higher fluorescence and more oxygenated waters. Thus it appears that while hydromedusae may have more closely tracked the plume's movements, larval fishes, copepods, and siphonophores were more variably dispersed throughout this well-mixed plume water mass.

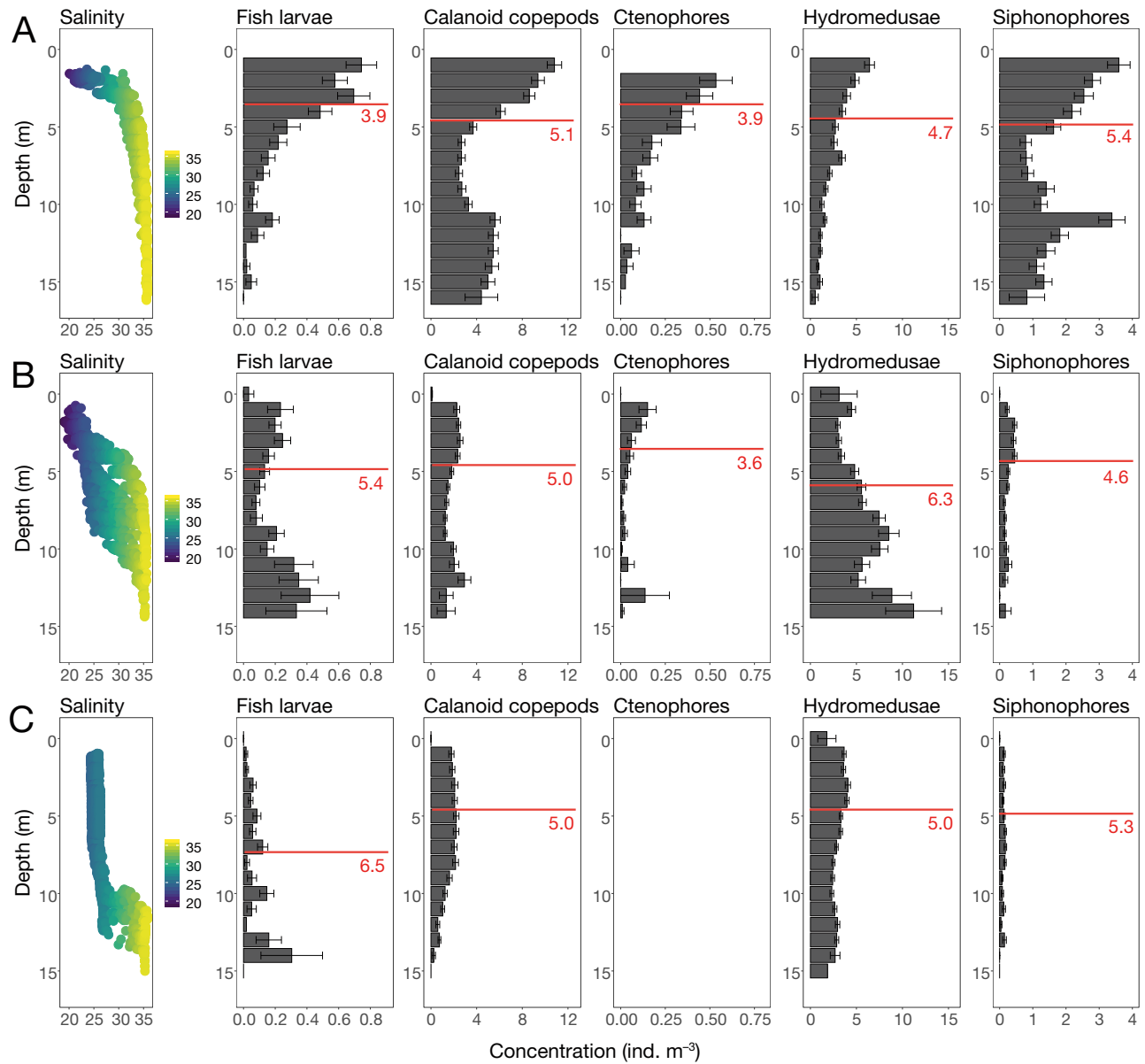


Fig. 6. Mean \pm SE concentrations (ind. m^{-3}) of each taxon category per 1 m depth bin in (A) stratified, (B) slightly-mixed, and (C) well-mixed transects, with transect salinity profiles shown in the far left column. Note the changing x-axis scale among the different taxa. All physical and biological data were collected by the ISIS between 9 and 11 April 2016. Red lines indicate the weighted mean depth (WMD; in meters) of taxa distributions

3.4. Predator–prey spatial relationships

Spearman correlation coefficients were also used to examine the spatial overlap of larval fishes with different prey and predator categories across the 3 plume regimes. In the stratified, more stable plume regime, fish larvae were significantly and positively correlated with their calanoid copepod prey and all categories of gelatinous predators ($p < 0.01$; Fig. 8A). As the volume of brackish water entering the Alabama continental shelf increased in the slightly-mixed plume regime, fish larvae remained significantly correlated

with their copepod prey ($p < 0.0001$) but became slightly less spatially correlated (though still significantly so) with ctenophores ($p < 0.01$) and siphonophores ($p < 0.01$) and not significantly correlated with hydromedusae ($p = 0.82$; Fig. 8B). In the well-mixed plume regime, where downwelling, strong currents, and turbulence affected $\sim 80\%$ of the water column, fish larvae were not significantly spatially correlated with either their prey or predators ($p > 0.01$; Fig. 8C). In other words, as wind-forcing, turbulence intensity, water column mixing, and advection processes strengthened, the spatial overlap among organisms decreased.

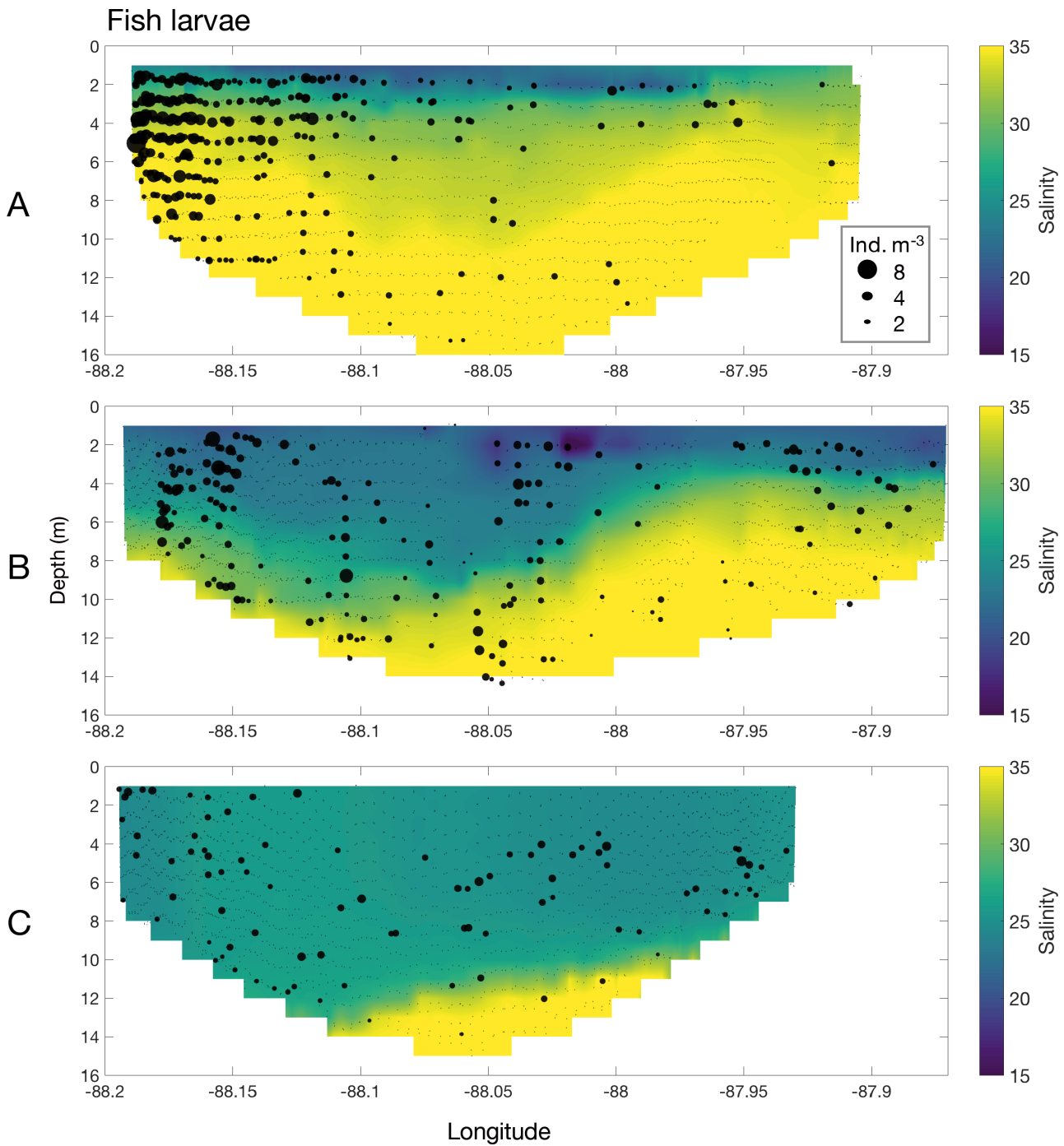


Fig. 7. Fine-scale distributions showing the aggregated concentrations (ind. m^{-3}) of key taxa for (A–C) fish larvae, (D–F) calanoid copepods, (G–I) ctenophores, (J–L) hydromedusae, and (M–O) siphonophores imaged by the ISIIS during sampling of the stratified (9 April; top panel in each plot), slightly-mixed (9–10 April; center panel), and well-mixed (10–11 April; bottom panel) plume regimes. Each point corresponds to the concentration of individuals within that 1 m sampling bin. Note the change in scale range among different biological categories. No ctenophores were captured in the well-mixed plume regime on 10–11 April 2016

(continued on next pages)

4. DISCUSSION

River plumes encountering shelf seas create complex nearshore dynamics. Analyses of the fine-scale

(1 m) vertical and horizontal spatial distributions of larval fishes and their zooplankton prey and predators enabled a comprehensive examination of the changes in overall abundances and spatial correlations among

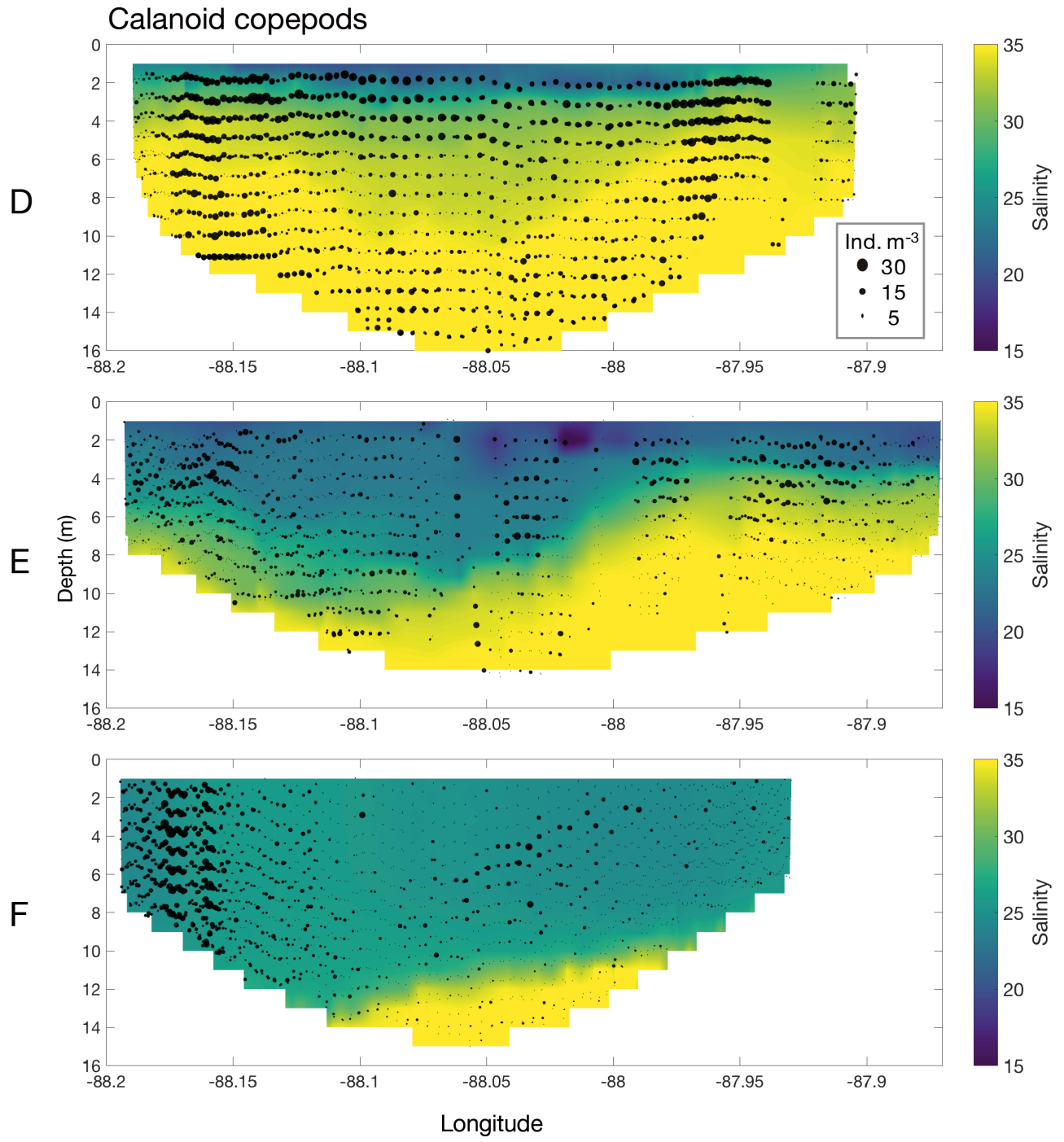


Fig. 7. (continued)

organisms across different regimes of wind-stress and mixing in a highly dynamic river plume system. While it is well-established that mesoscale frontal features cause major variations in physical oceanography and the distributions of organisms (e.g. Kiørboe et al. 1988, Munk et al. 2002, Lee et al. 2005), the use of an *in situ* plankton imager allowed for a substantially higher-resolution investigation of river plume processes than has previously been possible.

4.1. Larval fish distributions and predator–prey relationships across different plume regimes

High frequency, fine-scale sampling during a high river discharge event revealed the formation and dissipation of a multi-taxon biological aggregation over very short time scales. This aggregation was driven by a combination of plume-derived convergence, wind-induced downwelling, and advective

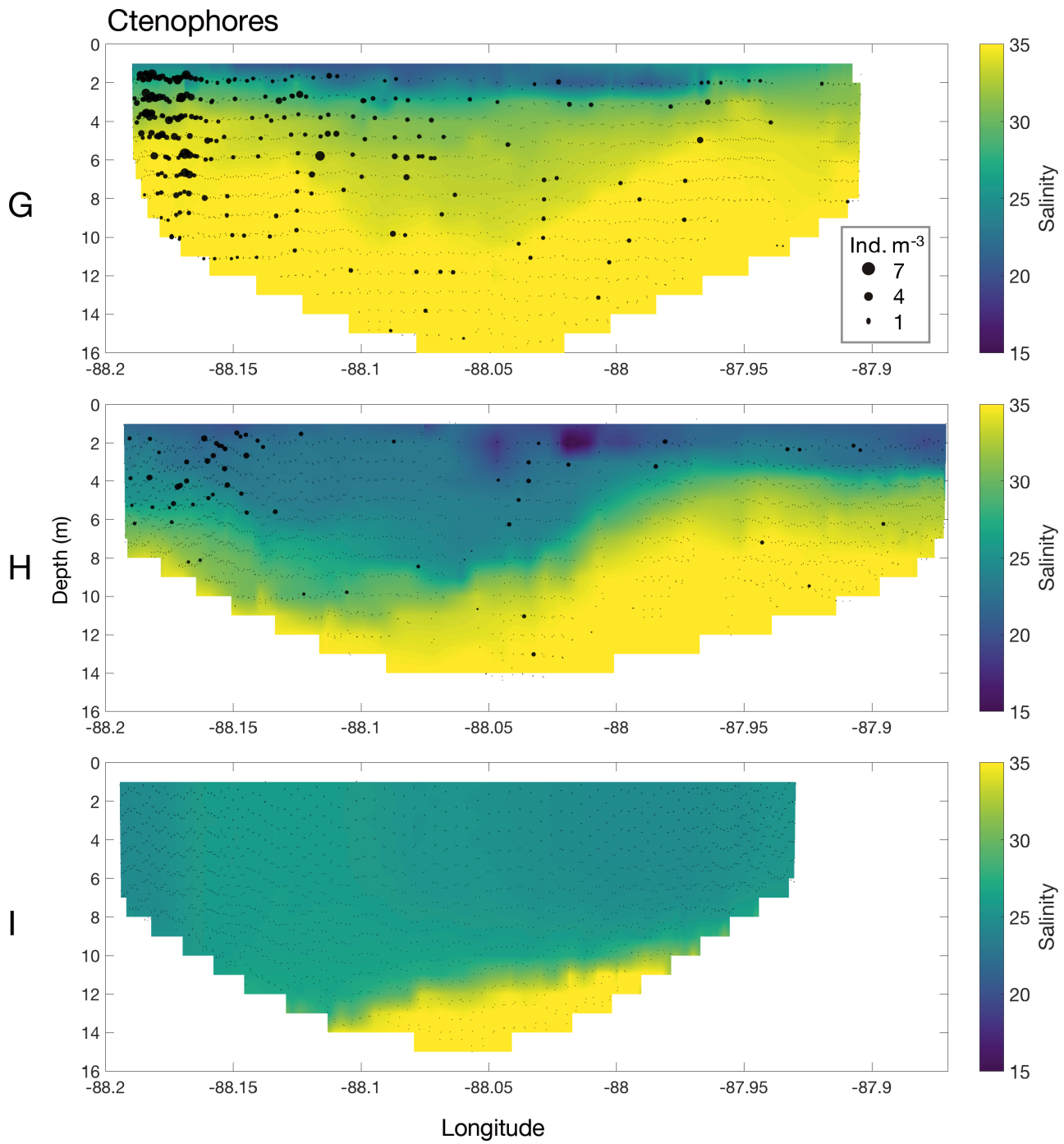


Fig. 7. (continued)

processes. Previous studies have documented elevated concentrations of larval fish and zooplankton near coastal river plumes (Govoni et al. 1989, Grimes & Finucane 1991, Morgan et al. 2005), yet the high spatiotemporal resolution of our sampling enables further insight into the physical processes responsible for the extreme variability of these biological phenomena. For example, the use of drifters provided real-time observations of the Mobile Bay plume

movements and enabled interpretations of why the highest biomass in our study period occurred during low-wind, stratified conditions on the 'downstream' side (west) of the Mobile Bay plume. The observed plankton aggregation was likely a result of the hydrodynamic convergence of an ebb tidal plume with alongshore currents and ambient shelf waters, causing a retention of fish larvae, zooplankton, and drifters.

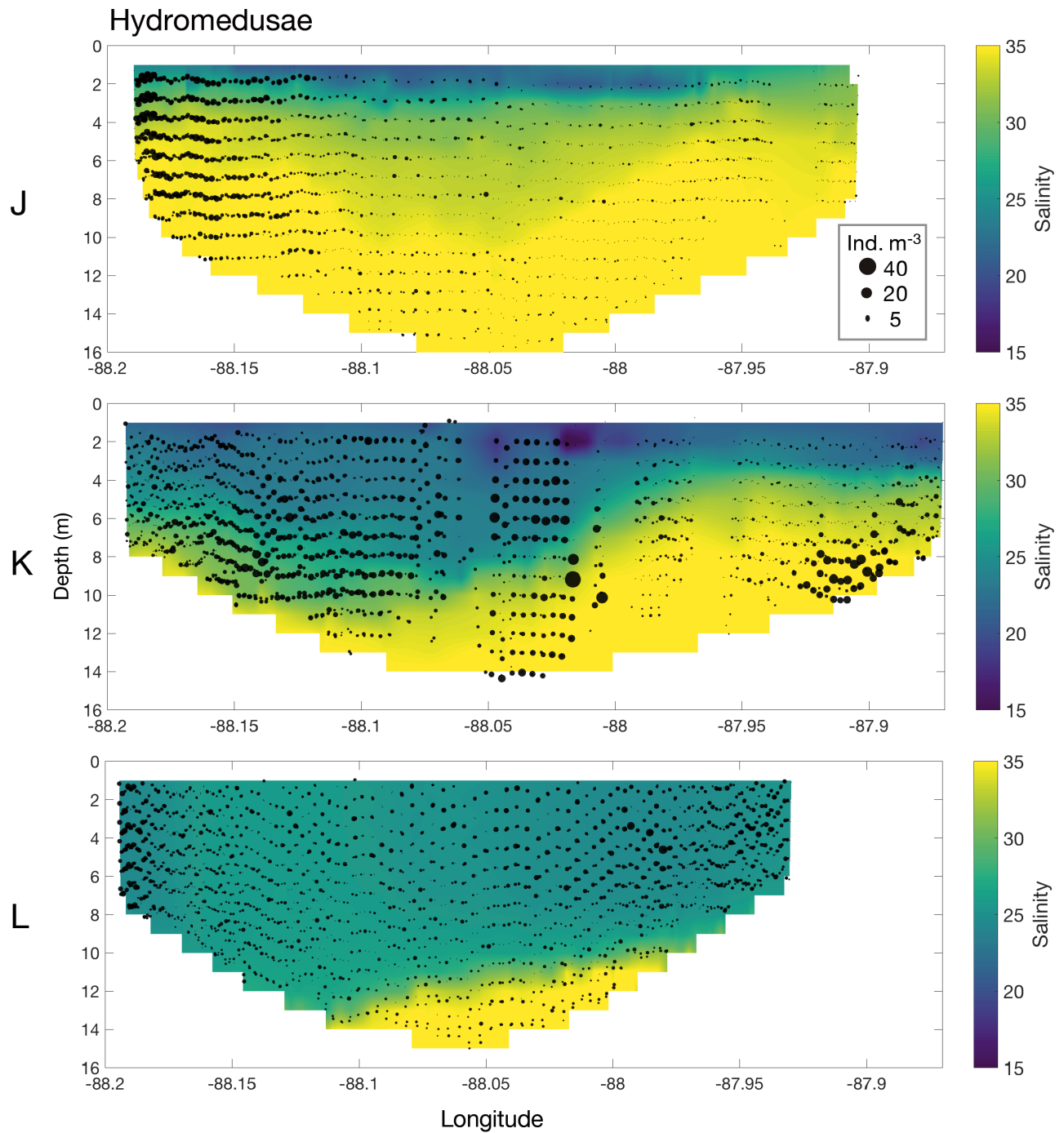


Fig. 7. (continued)

In these low-wind and stratified conditions, we observed high spatial correlations of fish larvae with calanoid copepods, a key prey item that both engraulids and sciaenids (the 2 most abundant fish families in the study region) are known to consume (McNeil & Grimes 1995, Holt & Holt 2000, Axler 2019). Because spatial overlap with prey is ultimately required for successful feeding, this documented overlap likely provides abundant feeding

opportunities for fish larvae distributed near the Mobile Bay plume outflow in both stratified and mixed conditions. In a companion study, larval striped anchovy and sand seatrout collected at a station near the western end of the stratified ISIIS transect on 9 April 2016 were analyzed for condition (via morphometric analysis) and growth (otolith microstructure). For both species, larvae from high salinity water masses (>32) were fatter at length and

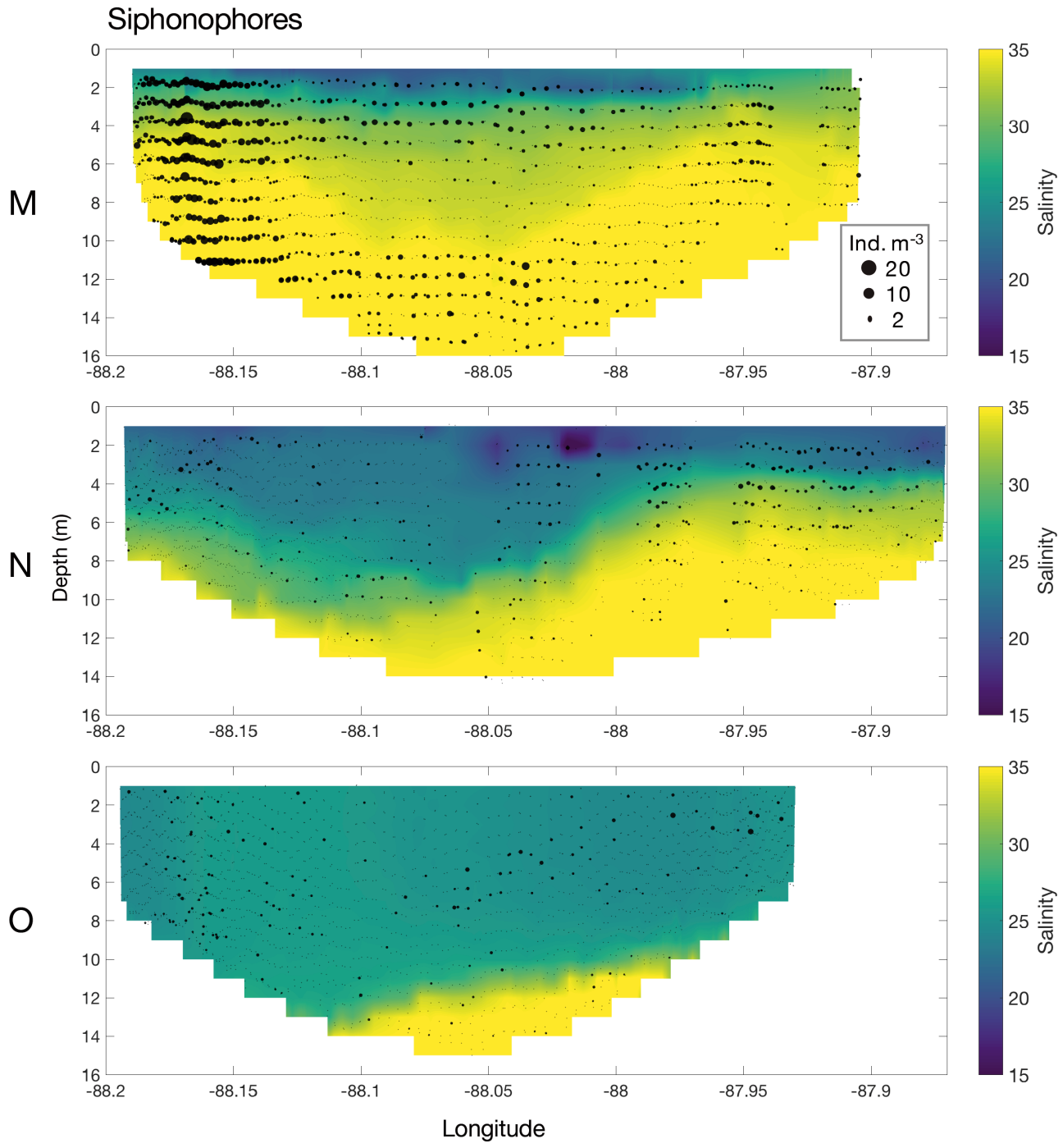


Fig. 7. (continued)

grew significantly faster over the last 3 d of life than conspecifics from within the plume water mass (≤ 25 salinity) farther east of this convergence region (Axler et al. 2020, this Theme Section). These data demonstrate that high feeding success was occurring in the same spatial and temporal location where fish larvae overlapped with their calanoid copepod prey. Spatial overlap, in this case caused by physical retention within a plume-derived con-

vergent region, ultimately led to successful predator-prey interactions, feeding, and larval growth.

Fish larvae also showed a high degree of spatial correlation with gelatinous zooplankton predators at the western end of the stratified transect, suggesting the potential for high predation pressure in these conditions. Hydromedusae, in particular, increased in biomass throughout this high discharge event and were widely prevalent throughout the water column.

This is not surprising, considering that gelatinous zooplankton are known to aggregate along density discontinuities (Graham et al. 2001, Bakun 2006). However, given the fairly high abundances of larval fishes near these high concentrations of gelatinous zooplankton, it seems probable that the larvae have some ability to avoid these tactile predators.

Over the following days, high river discharge produced a large plume pulse that moved through the study region and, when subjected to strong winds and turbulence, caused much of the inner shelf water column to mix. Our study revealed that biological taxa became less abundant and more deeply distributed as wind-forcing increased and the system changed to downwelling. It is possible that some of the larger, stronger-swimming organisms were capable of actively migrating out of the plume water mass, while smaller, less motile individuals were transported out of the survey region by the advective processes modifying the plume structure and location. Regardless of whether the mechanism was biological or physical, strong currents and water column turbulence, amplified by the large discharge event, dispersed the planktonic aggregation, reducing the probability of larval contact with both prey and predators, thus simultaneously creating a poor feeding environment but a potential refuge from predators. There may be an ecological ‘sweet spot’ here, wherein a stratified water column under enough plume influence and microturbulence to facilitate larval encounter with prey (e.g. ‘plankton contact hypothesis’; Rothschild & Osborn 1988, MacKenzie & Kiørboe 1995, MacKenzie 2000) is combined with high enough turbulence and fast-flowing currents to reduce predation by poorly-swimming, tactile gelatinous predators. However, conditions that decrease larval fish spatial overlap with their prey likely result in inadequate food resources for sufficient larval fish growth, potentially resulting in lower survival of larvae in those locations. During years when freshwater dis-

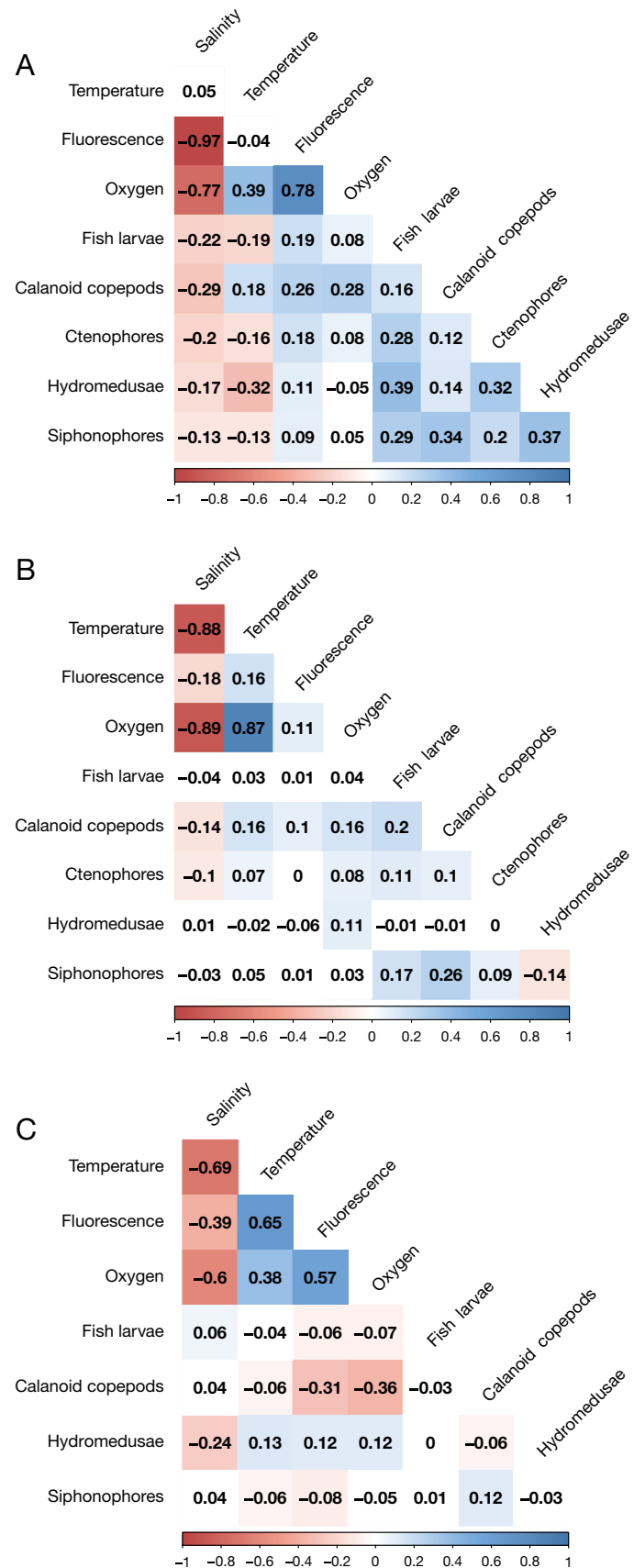


Fig. 8. Spearman correlation matrices for 1 m binned organism concentrations (ind. m^{-3}) and physical variables detected along full water column transects for: (A) stratified (9 April), (B) slightly-mixed (9–10 April), and (C) well-mixed (10–11 April) plume regimes. Correlation coefficient values are given in each square; <1 indicates a strong negative correlation, 0 means there is no association between the 2 variables, and >1 indicates a strong positive correlation. Positive correlations are displayed in blue and negative correlations in red, and color intensity is proportional to the correlation coefficient. Correlations with $p > 0.01$ were considered insignificant and left blank (white). No ctenophores were captured in the well-mixed plume regime on 10–11 April 2016

charge is anomalously high for long periods of time, this mechanism may contribute to a reduced number of recruits joining the adult population, an outcome that remains to be tested. Measuring the success of such cohorts would entail sustained high-resolution *in situ* sampling combined with individual growth analyses and cohort tracking, together a substantial research endeavor. Short of such an extensive collaborative study, results of the present study are a first step towards improving our understanding of larval fish survival under different plume regimes. Further, these observations underscore the extreme spatio-temporal variability in the physical (hydrographic gradients, currents, turbulence) and biological (predator-prey spatial overlap) environment relevant to individual fish larvae and inherent to river-dominated ecosystems, reiterating the need to study both the biology and the physics of these systems at much finer scales (and over more extensive domains) than has previously been done.

4.2. Implications for retention and dispersal of plankton in river-dominated coastal ecosystems

Aside from their high biological productivity, river plumes are thought to play an important role in fish population dynamics and recruitment by providing pathways for nearshore retention and dispersal of fish eggs and larvae. For example, river plumes have been observed transporting young stages into or away from estuarine nursery areas (Nelson et al. 1977, Shaw et al. 1985) or areas of recruitment to adult stocks (Power 1986). Eggs and early larvae can be transported by river discharge from spawning grounds to nursery habitats or, depending on the prevailing circulation patterns and physical forcing, away from favorable habitat before larvae have fully developed—thereby negatively impacting recruitment, as has been observed with larval gulf menhaden *Brevoortia patronus* (Govoni 1997) and juvenile Atlantic croaker *Micropogonias undulatus* (Carassou et al. 2011). In this way, it is thought that survival in some systems may be more transport-constrained than food-limited (Parrish et al. 1981).

Analysis of plume-tracking drifter tracks revealed multiple pathways for nearshore larval retention and dispersal near the mouth of Mobile Bay, including hydrodynamic convergence, wind-stress, horizontal advection, and micro-scale turbulence. Hydrodynamic convergence has long been thought to accumulate fish larvae and zooplankton within river plume frontal zones in a variety of systems, including

the Mississippi River (Govoni et al. 1989), Columbia River (Morgan et al. 2005), and Rhône River (Sabatés 1990). Not only does it increase spatial overlap of zooplankton and thus provide potentially favorable feeding environments as noted above, but it can also serve as an important retention mechanism for coastal-spawning species that use the inner shelf or adjacent estuary as nursery grounds (Govoni et al. 1989, Govoni & Grimes 1992). However, mechanisms of retention and dispersal can differ greatly among different river plume systems and physical forcing conditions. While we observed maximum concentrations of organisms on the ‘downstream’ side of a surface-adverted plume, Tilburg et al. (2007) observed patches of larval blue crabs *Callinectes sapidus* aggregating on the ‘upstream’ side of a Delaware Bay (USA) plume characterized by weak subtidal circulation and little buoyancy-driven forcing. The authors concluded that blue crab larvae appear to use these coastal null zones to maintain their position nearshore. Therefore, depending on the hydrodynamics of the system and prevailing oceanographic conditions, there may be multiple pathways that favor larval retention within productive inner shelf regions.

Due to the shallow nature of the Alabama continental shelf, wind can also cause dramatic changes in the structure and location of the plume, as evidenced by the complete reversal of the seaward-moving drifters during strong southeast winds on 10–11 April that pushed surface waters against the Alabama coast. Over the same time period, concentrations of larval fish and zooplankton (with the notable exception of hydromedusae) were reduced in the upper water column, likely because the water masses they resided in were pushed shoreward and replaced with plankton-poor water masses. The landward advection of the offshore extension of the plume after the transition from upwelling to downwelling favorable winds is a well-known nearshore retention mechanism that has previously been described for the Alabama continental shelf (Dzwonkowski et al. 2015) as well as for other systems such as the Columbia River plume (Hickey et al. 2005, Horner-Devine 2009). Depending on the tidal cycle and prevailing wind conditions, plankton residing near the bottom of the water column can be exposed to a different set of physical forces than plankton near the surface. At the same time that southeast winds caused downwelling of surface waters, deeper water masses continued moving seaward. Thus, while surface plankton were pushed rapidly shoreward (nearshore retention mechanism), deeper plankton were advected offshore (dispersal

mechanism). A previous study of the planktonic eggs of striped anchovy and drum (Sciaenidae) found that variability in the distribution of eggs was driven by the magnitude of river discharge, ambient circulation patterns in the region, and spawning location of the adults (Marley 1983). Despite the seaward flow of plume water near the surface, a net landward movement of denser, coastal shelf water along the bottom resulted in the retention of fish eggs spawned in and around the mouth of Mobile Bay (Marley 1983). Temperate fishes, particularly those that prey upon zooplankton, frequently spawn near mesoscale (20–200 km) oceanographic features such as river plumes, eddies, and other frontal zones potentially to directly release larvae in regions that support high prey concentrations (Kiørboe et al. 1988, Munk et al. 1999, Richardson et al. 2009). Upon hatching, larvae may use behavioral responses (e.g. vertical or horizontal swimming; Rijnsdorp et al. 1985, Epifanio 1988, Paris & Cowen 2004) to take advantage of favorable currents at different depths (e.g. tidal actions, shoreward currents underlying river plumes) to stay near suitable nursery habitats or otherwise reduce dispersive losses away from highly productive nearshore regions. Therefore, depending on ontogenetic stage and prevailing physical conditions, behavior may play a more critical role in the nearshore retention of fish larvae in river-dominated coastal ecosystems.

While the physical processes discussed so far produce conditions that retain and aggregate larval fishes and zooplankton near river systems, wind-forcing and shear between water masses can create turbulence capable of breaking down aggregations of zooplankton, mixing the water column, and dispersing individuals. In this study, we observed the rapid formation and dissipation of a plankton aggregation. While this was likely in part due to the horizontal advective processes discussed above, turbulence dissipation rates over the entire water column increased 3-fold from the first transect to the third transect. Over the same period of time, fish larvae transitioned from being spatially correlated with all prey and predator categories in the first transect to spatially correlated with no other taxa by the third transect. This disruption of biological aggregations is similar to the effects of internal waves on dense aggregations of larval fishes and their copepod prey off of Stellwagen Bank, Massachusetts (Greer et al. 2014). By mixing the stratified water column and forcing larval fishes into deeper water, the passage of internal waves reduced the spatial overlap between fish larvae and copepods while increasing

their overlap with the more deeply distributed gelatinous zooplankton predators. Because of the disrupting effect that turbulence has on fine-scale planktonic distributions and the transport of organisms to areas of favorable or unfavorable prey and predator encounters, tidal- or wind-driven turbulence is often considered an important factor affecting fish recruitment. For example, by increasing encounter rates of larval fishes with their planktonic prey, micro-scale turbulence in the water column has been considered to be critical to larval fish survival (Rothschild & Osborn 1988). Consistent with other studies (Munk & Kiørboe 1985, MacKenzie et al. 1994, Greer et al. 2014), our results suggest that low levels of turbulence in the pelagic environment enhance larval fish prey contact and potentially feeding up to a certain point, until turbulence becomes too strong and disperses normally persistent aggregations of prey.

Although biological distributions in our study are interpreted with regard to the effects of physical forcing, behavior may also contribute to these distributions. It is possible that the observed vertical distributions of taxa may have been partially influenced by nocturnal or reverse diel vertical migration (DVM) behaviors, wherein organisms migrate upward at dusk and downward at dawn or vice versa, respectively. Previous studies using acoustic backscatter measurements have shown that zooplankton vertical migrations change in a variety of ways in response to the presence of river plumes and stratification (Pearre 2003, Sindlinger et al. 2005). For instance, Parra et al. (2019) hypothesized that the strong halocline of a deepening Mississippi River plume can act as barrier for some vertically migrating zooplankton. However, we did not detect DVM behaviors despite the fact that ISIIS was undulated from near-surface to near-bottom through the entire water column. Further, due to the shallow nature of the Alabama shelf and our observations of the strength and degree of influence of the physical forcing (i.e. wind, river discharge, turbulence) and circulation patterns (i.e. ebb tidal plumes, coastal currents) dominating the water column, oceanographic features likely play a much larger role in structuring larval fish and zooplankton distributions than DVM-induced swimming behavior alone in this region. Ultimately, mapping the flow patterns and physical characteristics of these dynamic, river-influenced shelf regions and examining the fine-scale distributions of fish larvae across these regions is critical to understanding different dispersal and retention pathways for fish larvae in and around these highly variable environments.

5. CONCLUSIONS

Fine-scale (1 m) spatial relationships provide insights into how river plumes structure larval fish distributions and their predator–prey relationships, with the variability in distributions largely driven by the degree of wind-stress, magnitude of brackish water discharge, and ambient circulation patterns in the region. Previous studies have found that fisheries production is generally higher in coastal river-influenced ecosystems than in regions not under freshwater influence (Moore et al. 1970, Sánchez-Gil et al. 2008). Our analysis of *in situ* biological distributions with concurrent, high-resolution descriptions of their physical environment has enabled a fine-scale examination of the mechanisms underlying such regional observations. The aggregation and retention of planktonic prey (copepods) in a stratified water column near the Mobile Bay plume suggests that under stable conditions with minimal wind-forcing, distribution near a coastal river plume could facilitate enhanced prey contact and thus increase survival of fish larvae. However, our documentation of the spatial separation of fish larvae from their prey with increasing wind-stress and turbulence indicates that this relationship can quickly change. Rapid shifts in the biophysical structure of the nearshore water column during high discharge events may negatively impact larval fish survival (see also Axler et al. 2020). Therefore, our results suggest that the environmental conditions inherent of a freshwater-influenced coastal region can indeed enhance larval fish survival via bottom-up processes (feeding), but if physical forcing in the system becomes overwhelming (in this case via wind-stress in conjunction with high river discharge) and begins to dominate biological interactions, the habitat can quickly become unfavorable for larval fishes.

Ultimately, the observed environmental variability inherent in this river-dominated region highlights how rapidly the trophic environment can shift from favorable to poor (abundant to scant prey supply; low to high predator contact) for fish larvae over relatively small vertical scales (~10 m) and short temporal scales (hours to days) depending on wind-forcing and advective regimes. In a system this dynamic, the precise location and timing of sampling plays a large role in the observed results. Due to the coarse resolution of most ichthyoplankton sampling, the extreme variability in a larval fish's biophysical environment is rarely documented at this level of resolution, which likely underlies the large body of contradictory literature on the subject of larval fish survival and mortality in freshwater-influenced regions around the

world. Future climate projections for the nGOM are variable and uncertain, but general global patterns portend increases in weather extremes such as heavy precipitation storms, anomalously high freshwater discharge events, and wind speeds (Coumou & Rahmstorf 2012, Bruyère et al. 2017, Zeng et al. 2019). Examining fine-scale biological patterns in response to real-time changes in variable estuarine–shelf processes and coastal physical forcing is a first step toward understanding how future climate scenarios will affect fisheries production in river-dominated coastal ecosystems worldwide.

Acknowledgements. We thank the captains and crews of RVs 'Point Sur' and 'Pelican' for their assistance during the CONCORDE field sampling campaigns. Thanks also to numerous PIs, post-docs, technicians, and graduate students for their involvement with CONCORDE cruise logistics, field data collection, and sample processing, especially A. Deary, C. Culpepper, O. Lestrade, A. Hoover, S. Muffelman, K. Heidenreich, K. Martin, I. Soto Ramos, B. Jones, J. Moum, P. Vutukur, C. Van Appledorn, and Oregon State University's Ocean Mixing Group. Special thanks to J. Luo for her contributions to developing, testing, and applying the automated image identification method and C. Sullivan from Oregon State University's Center for Genomic Research and Biocomputing for his efforts implementing the image processing pipeline. Data analyses were enhanced by discussions with A. Greer, K. Swieca, and M. Schmid. This research was made possible by a grant from the Gulf of Mexico Research Initiative and its contribution EcoFOCI-0944 to NOAA's Ecosystems and Fisheries-Oceanography Coordinated Investigations Program. Raw collection data are available through the Gulf of Mexico Research Initiative Information & Data Cooperative (GRIIDC) at <https://data.gulfresearchinitiative.org> (drifter data: <https://doi.org/10.7266/N7TX3CFP>, Chameleon microstructure profiler data: <https://doi.org/10.7266/N7QF8R84>, ADCP data: <https://doi.org/10.7266/N77D2SJ5>, ISIIS raw physical data: <https://doi.org/10.7266/N79K48ND>, ISIIS binned taxa concentration data: <https://doi.org/10.7266/9211C8TM>).

LITERATURE CITED

- Axler KE (2019) Influence of river plumes on larval fish distributions, predator–prey relationships, and fitness in the northern Gulf of Mexico. MSc thesis, Oregon State University, Corvallis, OR
- Axler KE, Sponaugle S, Hernandez F Jr, Culpepper C, Cowen RK (2020) Consequences of plume encounter on larval fish growth and condition in the Gulf of Mexico. Mar Ecol Prog Ser 650:63–80
- Bakun A (2006) Fronts and eddies as key structures in the habitat of marine fish larvae: opportunity, adaptive response and competitive advantage. Sci Mar 70:105–122
- Bowman MJ, Iverson RL (1978) Estuarine and plume fronts. In: Bowman MJ, Esaias WE (eds) Oceanic fronts in coastal processes. Springer-Verlag, New York, NY, p 87–104
- Bruyère CL, Rasmussen R, Gutmann E, Done J and others (2017) Impact of climate change on Gulf of Mexico hurricanes. Tech Note NCAR/TN-5351STR. National Center

- for Atmospheric Research. <https://doi.org/10.5065/D6RN36J3>
- Carassou L, Dzwonkowski B, Hernandez FJ, Powers SP, Park K, Graham WM, Mareska J (2011) Environmental influences on juvenile fish abundances in a river-dominated coastal system. *Mar Coast Fish* 3:411–427
- Carassou L, Hernandez FJ, Powers SP, Graham WM (2012) Cross-shore, seasonal, and depth-related structure of ichthyoplankton assemblages in coastal Alabama. *Trans Am Fish Soc* 141:1137–1150
- Coumou D, Rahmstorf S (2012) A decade of weather extremes. *Nat Clim Chang* 2:491–496
- Cowan JLW, Pennock JR, Boynton WR (1996) Seasonal and interannual patterns of sediment-water nutrient and oxygen fluxes in Mobile Bay, Alabama (USA): regulating factors and ecological significance. *Mar Ecol Prog Ser* 141:229–245
- Cowen RK, Guigand CM (2008) *In Situ* Ichthyoplankton Imaging System (ISIIS): system design and preliminary results. *Limnol Oceanogr Methods* 6:126–132
- Cowen RK, Greer AT, Guigand CM, Hare JA, Richardson DE, Walsh HJ (2013) Evaluation of the *In Situ* Ichthyoplankton Imaging System (ISIIS): comparison with the traditional (bongo net) sampler. *Fish Bull* 111:1–12
- Dinnel SP, Schroeder WW, Wiseman WJ Jr (1990) Estuarine-shelf exchange using Landsat images of discharge plumes. *J Coast Res* 6:789–799
- Dykstra SL, Dzwonkowski B (2020) The propagation of fluvial flood waves through a backwater-estuarine environment. *Water Resour Res* 56:e2019WR025743
- Dzwonkowski B, Park K, Ha HK, Graham WM, Hernandez FJ, Powers SP (2011) Hydrographic variability on a coastal shelf directly influenced by estuarine outflow. *Cont Shelf Res* 31:939–950
- Dzwonkowski B, Park K, Lee J, Webb BM, Valle-Levinson A (2014) Spatial variability of flow over a river-influenced inner shelf in coastal Alabama during spring. *Cont Shelf Res* 74:25–34
- Dzwonkowski B, Park K, Collini R (2015) The coupled estuarine-shelf response of a river-dominated system during the transition from low to high discharge. *J Geophys Res Oceans* 120:6145–6163
- Dzwonkowski B, Fournier S, Park K, Dykstra S, Reager JT (2018a) Water column stability and the role of velocity shear on a seasonally stratified shelf, Mississippi Bight, Northern Gulf of Mexico. *J Geophys Res* 123:5777–5796
- Dzwonkowski B, Fournier S, Reager JT, Milroy S and others (2018b) Tracking sea surface salinity and dissolved oxygen on a river-influenced, seasonally stratified shelf, Mississippi Bight, northern Gulf of Mexico. *Cont Shelf Res* 169:25–33
- Epifanio CE (1988) Transport of crab larvae between estuaries and the continental shelf. In: Jansson BO (ed) *Coastal-offshore ecosystem interactions. Lecture Notes on Coastal and Estuarine Studies*, Vol 22. Springer, Berlin, p 291–305
- Failletaz R, Picheral M, Luo JY, Guigand C, Cowen RK, Irisson JO (2016) Imperfect automatic image classification successfully describes plankton distribution patterns. *Methods Oceanogr* 15–16:60–77
- Frost BW, Bollens SM (1992) Variability of diel vertical migration in the marine planktonic copepod *Pseudocalanus newmani* in relation to its predators. *Can J Fish Aquat Sci* 49:1137–1141
- Garvine RW, Monk JD (1974) Frontal structure of a river plume. *J Geophys Res Ocean Atmos* 79:2251–2259
- Gelfenbaum G, Stumpf RP (1993) Observations of currents and structure across a buoyant plume front density. *Estuaries* 16:40–52
- Govoni JJ (1997) The association of the population recruitment of Gulf menhaden, *Brevoortia patronus*, with Mississippi River discharge. *J Mar Syst* 12:101–108
- Govoni JJ, Chester AJ (1990) Diet composition of larval *Leiostomus xanthurus* in and about the Mississippi River plume. *J Plankton Res* 12:819–830
- Govoni JJ, Grimes CB (1992) The surface accumulation of larval fishes by hydrodynamic convergence within the Mississippi River plume front. *Cont Shelf Res* 12: 1265–1276
- Govoni JJ, Hoss DE, Colby DR (1989) The spatial distribution of larval fishes about the Mississippi River plume. *Limnol Oceanogr* 34:178–187
- Graham B (2015) Fractional max-pooling. arXiv:1412.6071v4
- Graham WM, Pagès F, Hamner WM (2001) A physical context for gelatinous zooplankton aggregations: a review. *Hydrobiologia* 451:199–212
- Greer AT, Cowen RK, Guigand CM, Hare JA, Tang D (2014) The role of internal waves in larval fish interactions with potential predators and prey. *Prog Oceanogr* 127:47–61
- Greer AT, Shiller AM, Hofmann EE, Wiggert JD and others (2018) Functioning of coastal river-dominated ecosystems and implications for oil spill response. *Oceanography* 31:90–103
- Grimes CB (2001) Fishery production and the Mississippi River discharge. *Fisheries* 26:17–26
- Grimes CB, Finucane JH (1991) Spatial distribution and abundance of larval and juvenile fish, chlorophyll and macrozooplankton around the Mississippi River discharge plume, and the role of the plume in fish recruitment. *Mar Ecol Prog Ser* 75:109–119
- Grimes CB, Lang KL (1992) Distribution, abundance, growth, mortality, and spawning dates of yellowfin tuna, *Thunnus albacares*, larvae around the Mississippi River discharge plume. *Collect Vol Sci Pap ICCAT Recl Doc Sci* 38:177–194
- Harrell FE Jr (2019) Hmisc: Harrell miscellaneous. R package version 4.2-0. <https://CRAN.R-project.org/package=Hmisc>
- Hernandez FJ, Powers SP, Graham WM (2010a) Detailed examination of ichthyoplankton seasonality from a high-resolution time series in the northern Gulf of Mexico during 2004–2006. *Trans Am Fish Soc* 139:1511–1525
- Hernandez FJ, Powers SP, Graham WM (2010b) Seasonal variability in ichthyoplankton abundance and assemblage composition in the northern Gulf of Mexico off Alabama. *Fish Bull* 108:193–207
- Hickey B, Geier S, Kachel N, McFadgen A (2005) A bi-directional river plume: the Columbia in summer. *Cont Shelf Res* 25:1631–1656
- Hjort J (1926) Fluctuations in the year classes of important food fishes. *J Cons Perm Int Explor Mer* 1:5–38
- Holt GJ, Holt SA (2000) Vertical distribution and the role of physical processes in the feeding dynamics of two larval sciaenids *Sciaenops ocellatus* and *Cynoscion nebulosus*. *Mar Ecol Prog Ser* 193:181–190
- Horner-Devine AR (2009) The bulge circulation in the Columbia River plume. *Cont Shelf Res* 29:234–251
- Houde ED (2002) Mortality. In: Fuiman LA, Werner RG (eds) *Fishery science. The unique contributions of early life stages*. Blackwell, Oxford, p 64–87

- Hu Q, Davis C (2006) Accurate automatic quantification of taxa-specific plankton abundance using dual classification with correction. *Mar Ecol Prog Ser* 306:51–61
- Kim CK, Park K (2012) A modeling study of water and salt exchange for a micro-tidal, stratified northern Gulf of Mexico estuary. *J Mar Syst* 96–97:103–115
- Kiørboe T, Munk P, Richardson K, Christensen V, Paulsen H (1988) Plankton dynamics and larval herring growth, drift and survival in a frontal area. *Mar Ecol Prog Ser* 44: 205–219
- Lang KL, Grimes CB, Shaw RF (1994) Variations in the age and growth of yellowfin tuna larvae, *Thunnus albacares*, collected about the Mississippi River plume. *Environ Biol Fishes* 39:259–270
- Le Fèvre J (1987) Aspects of the biology of frontal systems. *Adv Mar Biol* 23:163–299
- Le Pape O, Chauvet F, Désaunay Y, Guérault D (2003) Relationship between interannual variations of the river plume and the extent of nursery grounds for the common sole (*Solea solea*, L.) in Vilaine Bay. Effects on recruitment variability. *J Sea Res* 50:177–185
- Lee O, Nash RDM, Danilowicz BS (2005) Small-scale spatio-temporal variability in ichthyoplankton and zooplankton distribution in relation to a tidal-mixing front in the Irish Sea. *ICES J Mar Sci* 62:1021–1036
- Lohrenz SE, Fahnenstiel GL, Redalje DG, Lang GA, Chen X, Dagg MJ (1997) Variations in primary production of northern Gulf of Mexico continental shelf waters linked to nutrient inputs from the Mississippi river. *Mar Ecol Prog Ser* 155:45–54
- Luo JY, Grassian B, Tang D, Irisson JO and others (2014) Environmental drivers of the fine-scale distribution of a gelatinous zooplankton community across a mesoscale front. *Mar Ecol Prog Ser* 510:129–149
- Luo JY, Irisson JO, Graham B, Guigand C, Sarafraz A, Mader C, Cowen RK (2018) Automated plankton image analysis using convolutional neural networks. *Limnol Oceanogr Methods* 16:814–827
- MacKenzie BR (2000) Turbulence, larval fish ecology and fisheries recruitment: a review of field studies. *Oceanol Acta* 23:357–375
- MacKenzie BR, Kiørboe T (1995) Encounter rates and swimming behavior of pause-travel and cruise larval fish predators in calm and turbulent laboratory environments. *Limnol Oceanogr* 40:1278–1289
- MacKenzie BR, Miller T, Cyr S, Leggett WC (1994) Evidence for a dome-shaped relationship between turbulence and larval fish ingestion rates. *Limnol Oceanogr* 39:1790–1799
- Marley RD (1983) Spatial distribution patterns of planktonic fish eggs in lower Mobile Bay, Alabama. *Trans Am Fish Soc* 112:257–266
- McClatchie S, Cowen R, Nieto K, Greer A and others (2012) Resolution of fine biological structure including small narcomedusae across a front in the Southern California Bight. *J Geophys Res* 117:C04020
- McNeil CS, Grimes CB (1995) Diet and feeding ecology of striped anchovy, *Anchoa hepsetus*, along environmental gradients associated with the Mississippi River discharge plume. In: Atwood DK, Graham WF, Grimes CB (eds) Nutrient-enhanced coastal ocean productivity. Proceedings of the April 1994 Synthesis Workshop, Baton Rouge, Louisiana. Louisiana Sea Grant College Program, Baton Rouge, LA, p 81–89
- Moore D, Brusher HA, Trent L (1970) Relative abundance, seasonal distribution, and species composition of demersal fishes off Louisiana and Texas, 1962–1964. *Contrib Mar Sci* 15:45–70
- Morgan CA, De Robertis A, Zabel RW (2005) Columbia River plume fronts. I. Hydrography, zooplankton distribution, and community composition. *Mar Ecol Prog Ser* 299:19–31
- Moum JN, Gregg MC, Lien RC, Carr ME (1995) Comparison of turbulence kinetic energy dissipation rate estimates from two ocean microstructure profilers. *J Atmos Ocean Technol* 12:346–366
- Munk P, Kiørboe T (1985) Feeding behaviour and swimming activity of larval herring (*Clupea harengus*) in relation to density of copepod nauplii. *Mar Ecol Prog Ser* 24:15–21
- Munk P, Larsson PO, Danielsen DS, Moksness E (1999) Variability in frontal zone formation and distribution of gadoid fish larvae at the shelf break in the northeastern North Sea. *Mar Ecol Prog Ser* 177:221–233
- Munk P, Wright PJ, Pihl NJ (2002) Distribution of the early larval stages of cod, plaice and lesser sandeel across haline fronts in the North Sea. *Estuar Coast Shelf Sci* 55: 139–149
- Nelson WR, Ingham MC, Schaaf WE (1977) Larval transport and year-class strength of Atlantic menhaden, *Brevoortia tyrannus*. *Fish Bull* 75:23–41
- Ogle DH, Wheeler P, Dinno A (2020) FSA: fisheries stock analysis. R package version 0.8.27, <https://github.com/droglenc/FSA>
- Olson DB, Backus RH (1985) The concentrating of organisms at fronts: a cold-water fish and a warm-core Gulf Stream ring. *J Mar Res* 43:113–137
- Paris CB, Cowen RK (2004) Direct evidence of a biophysical retention mechanism for coral reef fish larvae. *Limnol Oceanogr* 49:1964–1979
- Parra SM, Greer AT, Book JW, Deary AL and others (2019) Acoustic detection of zooplankton diel vertical migration behaviors on the northern Gulf of Mexico shelf. *Limnol Oceanogr* 64:2092–2113
- Parrish RH, Nelson CS, Bakun A (1981) Biological oceanography transport mechanisms and reproductive success of fishes in the California Current. *Biol Oceanogr* 1:175–203
- Pearre S Jr (2003) Eat and run? The hunger/satiation hypothesis in vertical migration: History, evidence and consequences. *Biol Rev Camb Philos Soc* 78:1–79
- Peterson JO, Peterson WT (2008) Influence of the Columbia River plume (USA) on the vertical and horizontal distribution of mesozooplankton over the Washington and Oregon shelf. *ICES J Mar Sci* 65:477–483
- Powell AB, Chester AJ, Govoni JJ, Warlen SM (1990) Nutritional condition of spot larvae associated with the Mississippi River plume. *Trans Am Fish Soc* 119:957–965
- Power JH (1986) A model of the drift of northern anchovy, *Engraulis mordax*, larvae in the California Current. *Fish Bull* 84:585–603
- Purcell JE, Arai MN (2001) Interactions of pelagic cnidarians and ctenophores with fish: a review. *Hydrobiologia* 451: 27–44
- Core Team (2019) R: a language and environment for statistical computing. R Foundation for Statistical Computing, Vienna
- Reichert JM, Fryer BJ, Pangle K, Johnson TB, Tyson JT, Drelich AB, Ludsin SA (2010) River-plume use during the pelagic larval stage benefits recruitment of a lentic fish. *Can J Fish Aquat Sci* 67:987–1004
- Richardson DE, Llopiz JK, Leaman KD, Vertes PS, Muller-Karger FE, Cowen RK (2009) Sailfish (*Istiophorus platypterus*) spawning and larval environment in a Florida

- Current frontal eddy. *Prog Oceanogr* 82:252–264
- Rijnsdorp AD, Van Stralen M, Van Der Veer HW (1985) Selective tidal transport of North Sea plaice larvae *Pleuronectes platessa* in coastal nursery areas. *Trans Am Fish Soc* 114:461–470
- Rissik D, Suthers IM (1996) Feeding in a larval fish assemblage: the nutritional significance of an estuarine plume front. *Mar Biol* 125:233–240
- Rothschild BJ, Osborn TR (1988) Small-scale turbulence and plankton contact rates. *J Plankton Res* 10:465–474
- Sabatés A (1990) Changes in the heterogeneity of mesoscale distribution patterns of larval fish associated with a shallow coastal haline front. *Estuar Coast Shelf Sci* 30:131–140
- Sánchez-Gil P, Yáñez-Arancibia AY, Tapia M, Day JW, Wilson CA, Cowan JH (2008) Ecological and biological strategies of *Etropus crossotus* and *Citharichthys spilopterus* (Pleuronectiformes: Paralichthyidae) related to the estuarine plume, Southern Gulf of Mexico. *J Sea Res* 59:173–185
- Schroeder WW (1979) The dispersion and impact of Mobile River system waters in Mobile Bay, Alabama. Bull 37. Water Resources Research Institute, Auburn University, Auburn, AL
- Schroeder WW, Lysinger WR (1979) Hydrography and circulation in Mobile Bay. In: Loyacano HA, Smith JP (eds) Symposium on the natural resources of the Mobile Bay Estuary. U.S. Army Corps of Engineers, Mobile, AL, p 75–94
- Shaw RF, Wiseman WJ, Turner RE, Rouse LJ, Condrey RE, Kelly FJ (1985) Transport of larval Gulf menhaden (*Brevoortia patronus*) in continental shelf waters of western Louisiana: a hypothesis. *Trans Am Fish Soc* 114:452–460
- Sindlinger LR, Biggs DC, Dimarco SF (2005) Temporal and spatial variability of ADCP backscatter on a continental slope. *Cont Shelf Res* 25:259–275
- Stumpf RP, Gelfenbaum G, Pennock JR (1993) Wind and tidal forcing of a buoyant plume, Mobile Bay, Alabama. *Cont Shelf Res* 13:1281–1301
- Tilburg CE, Dittel AI, Epifanio CE (2007) Retention of crab larvae in a coastal null zone. *Estuar Coast Shelf Sci* 72: 570–578
- Turner RE, Rabalais NN (1991) Changes in Mississippi River water quality this century. *Bioscience* 41:140–147
- USGS (United States Geological Survey) (2016a) Alabama River at Claiborne Lock and Dam near Monroeville, Alabama. National Water Information System, USGS 02428400. http://waterdata.usgs.gov/usa/nwis/uv?site_no=02428400 (accessed January 2019)
- USGS (2016b) Tombigbee River at Coffeeville Lock and Dam, near Coffeeville, Alabama, National Water Information System, USGS 02469761. http://waterdata.usgs.gov/usa/nwis/uv?site_no=02469761 (accessed January 2019)
- Wickham H (2016) Ggplot2: elegant graphics for data analysis. Springer-Verlag, New York, NY
- Wickham H, François R, Henry L, Müller K (2018) Dplyr: a grammar of data manipulation. R package version 0.7.6. <https://CRAN.R-project.org/package=dplyr>
- Zeng Z, Ziegler AD, Searchinger T, Yang L and others (2019) A reversal in global terrestrial stilling and its implications for wind energy production. *Nat Clim Chang* 9:979–985

Editorial responsibility: Rebecca Asch (Guest Editor), Greenville, NC, USA

Submitted: October 21, 2019; *Accepted:* June 23, 2020
Proofs received from author(s): July 27, 2020